Neuron

Article

A latent pool of neurons silenced by sensory-evoked inhibition can be recruited to enhance perception

Graphical abstract

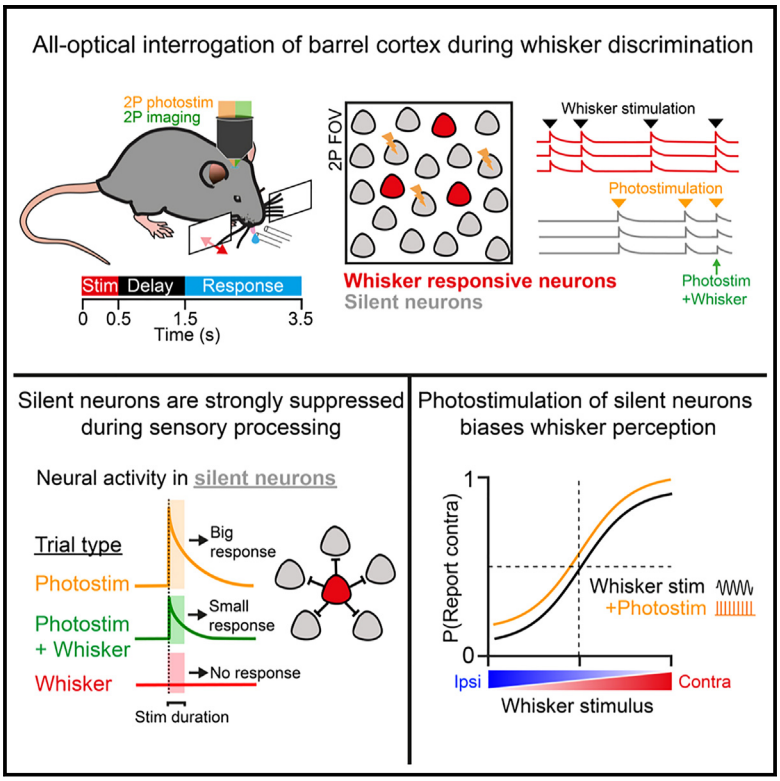

Highlights

- All-optical interrogation of barrel cortex during bilateral whisker discrimination
- Sparse coding of contralateral and ipsilateral whisker information
- Selective sensory-evoked inhibition helps ensure sparse coding
- Optogenetic recruitment of stimulus non-coding neurons can aid perception

Authors

Oliver M. Gauld, Adam M. Packer, Lloyd E. Russell, ..., Arnd Roth, Beverley A. Clark, Michael Häusser

Correspondence

o.gauld@ucl.ac.uk (O.M.G.), m.hausser@ucl.ac.uk (M.H.)

In brief

Gauld et al. use all-optical interrogation to probe sparse coding in the barrel cortex. They find that targeted photostimulation of task-silent neurons evokes perceptual choice bias and that these neurons are selectively suppressed by inhibition during whisker processing. Their findings show that silent neurons can be recruited to enhance behavior.

Gauld et al., 2024, Neuron *112*, 2386–2403
July 17, 2024
https://doi.org/10.1016/j.neuron.2024.04.015

CellPress

CellPress
OPEN ACCESS

Neuron

Article

A latent pool of neurons silenced by sensory-evoked inhibition can be recruited to enhance perception

Oliver M. Gauld,[1,2,*] Adam M. Packer,[1,3] Lloyd E. Russell,[1] Henry W.P. Dalgleish,[1] Maya Iuga,[1] Francisco Sacadura,[1] Arnd Roth,[1] Beverley A. Clark,[1] and Michael Häusser[1,4,*]

[1]Wolfson Institute for Biomedical Research, University College London, London WC1E 6BT, UK
[2]Sainsbury Wellcome Centre, University College London, London W1T 4JG, UK
[3]Department of Physiology, Anatomy and Genetics, University of Oxford, Oxford OX1 3PT, UK
[4]Lead contact
*Correspondence: o.gauld@ucl.ac.uk (O.M.G.), m.hausser@ucl.ac.uk (M.H.)
https://doi.org/10.1016/j.neuron.2024.04.015

SUMMARY

To investigate which activity patterns in sensory cortex are relevant for perceptual decision-making, we combined two-photon calcium imaging and targeted two-photon optogenetics to interrogate barrel cortex activity during perceptual discrimination. We trained mice to discriminate bilateral whisker deflections and report decisions by licking left or right. Two-photon calcium imaging revealed sparse coding of contralateral and ipsilateral whisker input in layer 2/3, with most neurons remaining silent during the task. Activating pyramidal neurons using two-photon holographic photostimulation evoked a perceptual bias that scaled with the number of neurons photostimulated. This effect was dominated by optogenetic activation of non-coding neurons, which did not show sensory or motor-related activity during task performance. Photostimulation also revealed potent recruitment of cortical inhibition during sensory processing, which strongly and preferentially suppressed non-coding neurons. Our results suggest that a pool of non-coding neurons, selectively suppressed by network inhibition during sensory processing, can be recruited to enhance perception.

INTRODUCTION

Understanding how sensory inputs are transformed into perceptual outputs requires functional dissection of cortical circuits during behavior.[1,2] Neural circuits in the superficial layers of the sensory cortex are largely composed of excitatory neurons that show heterogenous stimulus tuning,[3] structured patterns of connectivity,[4–8] and low spike rates.[9] GABAergic interneurons, which are densely connected with local excitatory neurons[10,11] and have high baseline firing rates[12] and broad receptive fields,[13] provide inhibition that patterns spatiotemporal excitation.[14–18] Accordingly, sensory processing in the superficial cortex is typically dominated by subsets of highly tuned neurons,[19–21] with most excitatory neurons remaining "silent" during behavior.[22,23]

The observation that few neurons are engaged during sensory processing and that their activity correlates with perceptual decisions[24–27] suggests the cortex uses a sparse neural code to generate stimulus percepts.[25,28,29] Sparse coding is an efficient mechanism for encoding information,[30–32] and has been observed experimentally across a range of neural systems.[33,34] In causal support of the sparse coding hypothesis, experimental stimulation of small groups of cortical neurons, and even single neurons, can elicit perceptual responses.[26,35–41] Moreover, functionally targeted microstimulation can also influence decisions in favor of the tuning of the manipulated neurons.[42–46]

As these findings indicate that perception is driven by small stimulus-tuned "ensembles," the functional significance of the large proportion of non-responsive neurons in the sensory cortex has remained enigmatic.[23,47,48] Neurons may appear silent if they have selective receptive fields that are not explored by standard experimental sensory stimulation paradigms.[33] Alternatively, non-responsive neurons may be reserved for implementing circuit plasticity.[22,49] Understanding why so few neurons respond strongly to sensory stimuli and how such sparse activity can drive reliable sensorimotor behavior is fundamental for understanding cortical circuit function.[21,50–52]

Here, we used simultaneous two-photon (2P) calcium imaging and holographic 2P photostimulation (PS)[53–56] to interrogate sparse coding in the barrel cortex while head-fixed mice performed a bilateral whisker discrimination task. We opted to probe barrel cortex under bilateral sensory conditions as bilateral processing is an ethological aspect of tactile sensation for subterranean rodents.[57–60] Moreover, perturbing barrel cortex impairs bilateral whisker tasks,[57,59,61] suggesting that bilateral somatosensation is barrel cortex-dependent. By characterizing the circuit response to paired whisker stimulation and patterned 2P PS, we provide new insights into the mechanistic basis of sparse coding and show that intrahemispheric perceptual signals can be enhanced by releasing "non-coding" L2/3 neurons from inhibition, consistent with

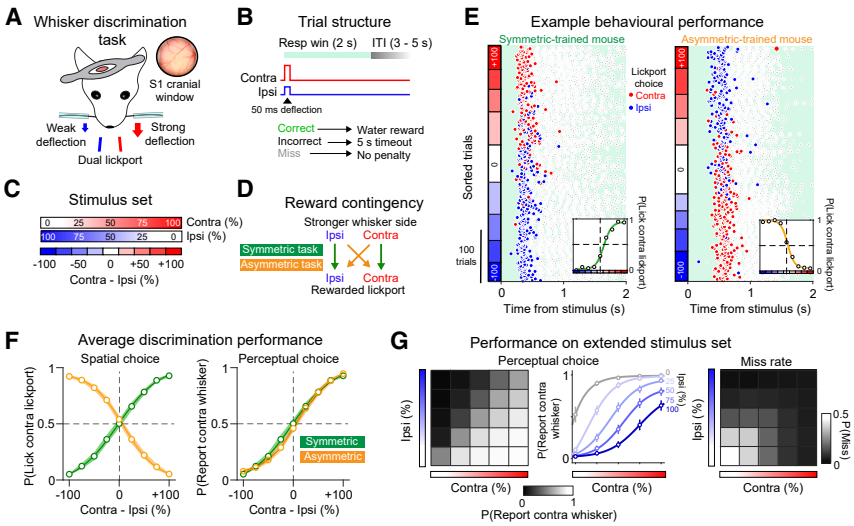

Figure 1. A whisker-guided task for graded bilateral intensity discrimination

(A) Whisker discrimination task setup. The inset shows an image of cortex through a 3 mm cranial window implanted over S1.

(B) Schematic of trial structure and trial outcome.

(C) "Cross-fading" bilateral whisker deflection stimulus design.

(D) Overview of symmetric (green) and asymmetric (orange) stimulus-reward contingencies.

(E) Example session performance from a symmetric-trained mouse (left) and an asymmetric-trained mouse (right). Trials were delivered in a randomized order but were sorted along the y axis according to stimulus difference as in (C). Each row corresponds to a trial, and each marker corresponds to a lick. The first lick is colored red/blue for contra/ipsi choice. The inset shows the session psychometric curve.

(F) Average psychometric performance for symmetric (green; $n = 31$ mice) and asymmetric (orange; $n = 30$ mice) trained mice. The left and right plots show spatial choice and perceptual choice tendency, respectively.

(G) Average performance during matrix stimulus sessions. Left: average P(Report contra whisker) is shown across trial types with each square in the 5 × 5 grid representing a different combination of contra and ipsi input. Middle: behavioral data are replotted such that each row in the left behavioral matrix (corresponding to a different ipsi stimulus level) is now shown as a psychometric curve. Right: average miss rate is shown across stimuli. Group data in Figure 1 are shown as the mean across mice, with error bars representing SEM.

work implicating silent cortical neurons in sensorimotor plasticity.[22,49]

RESULTS

A bilateral discrimination task for probing whisker perception

To probe the relationship between barrel cortex activity and stimulus perception, we developed a whisker discrimination task for head-fixed mice. First, we co-expressed the calcium indicator GCaMP6s and excitatory opsin C1V1 in barrel cortex neurons using a viral expression strategy (Figures S1A and S1B). During the task, the contralateral and ipsilateral C2 whiskers were simultaneously deflected, and mice discriminated the larger amplitude side and reported their choice with directional licking (Figures 1A–1C). We counterbalanced the stimulus-response contingency across mice (Figure 1D). Mice trained on the symmetric contingency learned a congruent spatial mapping between the stronger stimulus side and the target "lick" response (e.g., stim left → lick left), while mice trained on the asymmetric contingency learned the inverse rule (e.g., stim left → lick right). Mice learned the task structure through training on unilateral trials (Figures S2A and S2B). Performance was comparable across sides (Figure S2C) and contingencies (Figure S2D), although reaction times (RTs) were faster for symmetric-trained mice (Figure S2E). When using weaker stimuli, miss rate and RT increased (Figures S2F and S2G), and whisker-trimming abolished stimulus detection (Figure S2H). Unilateral muscimol infusion in barrel cortex selectively impaired contralateral trials (Figure S2I), indicating that performance requires both whisker input and barrel cortex.

Discrimination training yielded high-quality psychometric curves with large numbers of trials per session (309.1 ± 93.7 trials; mean ± SD; Figure 1E). Average psychometric curves from symmetric and asymmetric-trained cohorts of mice were inverted when we quantified spatial choice tendency as a function of stimulus difference (Figure 1F left), but comparable when we quantified the tendency mice would report the contralateral whisker stimulus (Figure 1F right). As the comparison between contingencies was not the primary focus of our study, we pooled data across contingencies unless otherwise stated. We trained some mice on an extended stimulus set comprising a larger combination of trial types (5 × 5 stimulus "matrix"; $n = 83$ sessions in 21 mice). Performance during these sessions demonstrates that mice solve the task by integrating stimuli bilaterally (Figure 1G). We also probed the temporal limits of bilateral discrimination (Figure S3A; $n = 58$ sessions in 25 mice). Temporal intervals led to strong choice biases that aligned with the leading stimulus side and saturated at 100 ms (Figures S3B and S3C). Temporal sensitivity appeared stronger in symmetric-trained mice (Figure S3D) and correlated with average RTs on whisker trials (Figure S3E). Together, our results demonstrate that the whisker system supports fine-scale discrimination of bilateral tactile input and that barrel cortex can generate stable sensory percepts within 100 ms of stimulus input to guide behavior.

Bulk optogenetic activation of the barrel cortex evokes a contralateral percept

Following learning, we photostimulated C1V1-expressing pyramidal neurons using an LED and measured whether a single optogenetic stimulus could "fool" mice into reporting a contralateral whisker deflection (Figure 2A). We calculated a "fooling index" as the difference in probability that optogenetic stimulation would evoke a contralateral vs. an ipsilateral whisker choice. Optogenetic stimulation of barrel cortex evoked illusory perceptual responses that increased with stimulation power (fooling

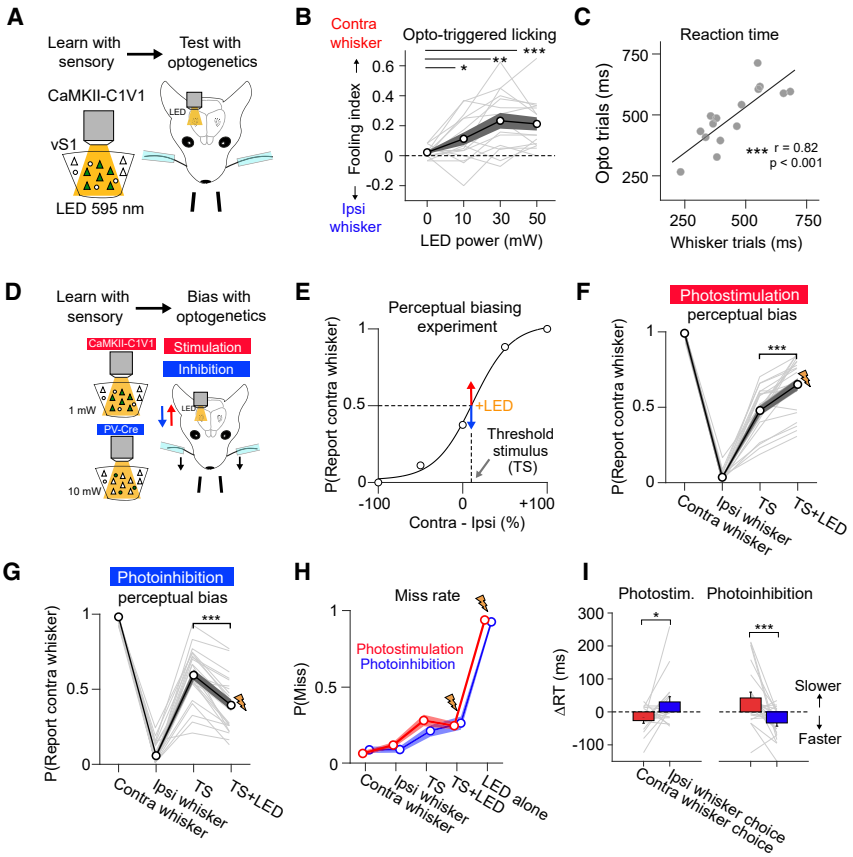

Figure 2. Optogenetic manipulation of barrel cortex during task performance

(A) Optogenetic "substitution" experiment schematic.

(B) Perceptual fooling index on optogenetic stimulation trials.

(C) Correlation between average reaction times on optogenetic stimulation trials (mean across 30 and 50 mW trials) and whisker trials. Each data point shows an individual session.

(D) Schematic of photostimulation (red) and photoinhibition (blue) perceptual biasing experiments.

(E) Optogenetic stimuli were paired with the bilateral whisker threshold stimulus (TS).

(F) Behavioral performance during photostimulation biasing experiments.

(G) Behavioral performance during photoinhibition biasing experiments.

(H) Miss rate is shown across trial types during photostimulation (red) and photoinhibition (blue) experiments.

(I) Optogenetic biasing of TS trial reaction time for photostimulation (left) and photoinhibition (right) experiments. The mean difference in RT on trials where mice reported the contralateral whisker choice vs. the ipsilateral whisker choice is shown as red and blue bars, respectively. Data in Figure 2 show the average across sessions as circular markers and SEM (shaded error bars). Data from individual sessions are shown as thin gray lines. All statistical tests were two-tailed Wilcoxon signed-rank tests * $p < 0.05$; ** $p < 0.01$; *** $p < 0.001$.

index: 0 mW = 0.02 ± 0.04; 10 mW = 0.11 ± 0.16; * $p = 0.047$; 30 mW = 0.23 ± 0.2; ** $p = 0.002$; 50 mW = 0.21 ± 0.17; *** $p = 6.1 \times 10^{-5}$; $n = 16$ sessions in 12 mice; Figure 2B). Optogenetic stimulation evoked contralateral licking in symmetric-trained mice but ipsilateral licking in asymmetric-trained mice (Figure S4A). Mean RT on whisker and LED trials were highly correlated (Pearson's correlation (r) = 0.82, *** $p = 0.0002$; Figure 2C), with faster LED-evoked RT measured in symmetric-trained mice (Figure S4B). LED-triggered licking was absent in control mice (Figure S4C). Our results therefore confirm that large-scale optogenetic activation of barrel cortex is sufficient to evoke contralateral whisker perception and initiate a goal-directed "action" specific to the learned sensorimotor context.[26,40]

Bidirectional optogenetic biasing of whisker choice

Next, we assessed whether optogenetically manipulating barrel cortex biased perceptual choice at the whisker discrimination threshold (Figure 2D). We first performed PS experiments using a low LED power estimated to have negligible *de novo* perceptual saliency (1 mW; Figure S4D). At the start of each experiment, we calibrated the whisker threshold stimulus (TS; Figure 2E). LED stimulation biased psychophysical reports on TS trials toward the contralateral whisker (ΔP[Report contra whisker] = 0.17 ± 0.13; *** $p = 1.1 \times 10^{-4}$; Wilcoxon signed-rank test; $n = 21$ sessions in 19 mice; Figure 2F), increasing contralateral lickport choices in symmetric-trained mice while increasing ipsilateral lickport choices in asymmetric-trained mice (Figure S4E). The effect was strongest when LED stimulation was delivered with a short delay relative to the TS (Figure S4F), which could reflect greater temporal coincidence between optogenetic and sensory-driven activity in cortex due to the short sensory signaling latency.

We then examined the effect of suppressing barrel cortex activity on choice tendency. We silenced barrel cortex by optogenetically activating (PV) interneurons expressing C1V1. Stimulation of PV interneurons simultaneously with TS input biased choice toward the ipsilateral whisker (ΔP[Report contra whisker] = −0.2 ± 0.11; *** $p = 2.7 \times 10^{-5}$; Wilcoxon signed-rank test; $n = 23$ sessions in 4 mice; Figure 2G). This effect decreased as a function of photoinhibition latency and was absent 100 ms after the TS (Figure S4G). During both PS and photoinhibition experiments, LED presentation did not change miss rate on TS trials (PS TS vs. TS+LED ΔP[Miss] = −0.034 ± 0.13, n.s. $p = 0.64$; photoinhibition ΔP[Miss] = 0.05 ± 0.13, n.s. $p = 0.09$) and did not evoke reliable licking responses when presented alone (P[Miss] on LED trials; PS = 0.94 ± 0.06; photoinhibition = 0.93 ± 0.08; Figure 2H).

Optogenetic manipulations also influenced RT (Figure 2I). PS of excitatory neurons decreased RT for contralateral whisker choices (ΔRT contra whisker choice = −26.4 ± 36.6 ms; ** $p = 0.004$; Wilcoxon signed-rank test), while also tending to increase RT for ipsilateral whisker choices (ΔRT ipsi whisker choice = 30.3 ± 72.1 ms;

n.s. $p = 0.08$; Figure 2I left). Photoinhibition of barrel cortex via activation of PV interneurons resulted in the inverse effect, increasing RT for contralateral whisker choices (ΔRT contra whisker choice = 42.3 ± 85.2 ms; * $p = 0.02$) while decreasing RT for ipsilateral whisker choices (ΔRT ipsi whisker choice = −33.6 ± 45.7 ms; ** $p = 0.004$; Figure 2I right). RT effects also decreased as a function of LED onset latency (Figure S4H). Together, our experiments show that unilateral PS and photoinhibition exert inverse and timing-dependent biases in perceptual decisions and perceptual speed within 100 ms from whisker deflection onset, indicating that barrel cortex plays a causal, but transient, role in perceptual processing during task performance.

2P imaging of the barrel cortex during delayed discrimination

To characterize task-related neural activity, we used 2P calcium imaging to record from GCaMP6s-expressing L2/3 neurons. As our initial experiments indicated that mice execute rapid decisions following whisker input, we developed a delayed-response version of the task to separate "sensation" and "action" epochs. To circumvent the requirement to trim the surrounding whiskers, we changed the stimulus effector from a glass capillary to a "paddle," which engaged multiple whiskers simultaneously (Figure 3A) and should also drive a larger stimulus-responsive neuronal population. To further increase stimulus saliency to aid performance in this more demanding task, the whiskers were deflected using sinusoidal waveforms that were fixed in frequency (20 Hz) but varied in amplitude bilaterally across trials. Thus, mice solved the task by discriminating deflection amplitude bilaterally, analogous to the single-whisker task (Figure 1). Following stimulus presentation (500 ms), mice withheld licking across a 1 s delay until cued to respond with an auditory cue. A motorized lickport was then translated into position to initiate the response window (Figure 3B).

We trained two groups of naïve mice on the symmetric and asymmetric version of this delayed-response task (Figures S5A–S5F). Moving the stimulus paddles out of reach of the whiskers reduced performance to chance (Figure S5G), confirming that mice do not use audio-visual cues to solve the task. Following learning, mice were trained on the 5 × 5 matrix stimulus set (Figure S5H). Discrimination performance was comparable to the cohort of mice trained on the non-delay task (Figure 1G), indicating that the underlying perceptual discrimination task is similar between the single-whisker non-delay and multi-whisker delay tasks. We then imaged L2/3 during task performance (Figure 3C) while using simultaneous videography to quantify task-evoked movement and licking (Figure S6; STAR Methods). The 2P imaging field-of-view (FOV) was targeted to the stimulus paddle-responsive region of barrel cortex based on widefield fluorescence maps (Figures S1C and S1D). As we did not find clear differences in neural responses across symmetric and asymmetric-trained mice (Figure S7), we pooled both datasets unless otherwise stated.

Sparse coding of whisker information in L2/3

To isolate sensory-evoked signals prior to licking, we analyzed stimulus-evoked fluorescence (ΔF/F) responses during the delay epoch (Figure 3B *green shading*; 500–1,000 ms post-stimulus). We first assessed whether neurons showed a preference for contra vs. ipsi unilateral input by using receiver operating characteristic (ROC) analysis to compute stimulus selectivity (area under the curve; AUC). This revealed a broad distribution of selectivity across the L2/3 population, with some neurons preferring contra trials (red neurons in Figure 3D; neurons 1 and 2 in Figure 3E), and others preferring ipsi trials (blue neurons in Figure 3D; neurons 3 and 4 in Figure 3E). Surprisingly, a comparable proportion of neurons were significantly selective for contra (fraction of all cells: 0.14 ± 0.05 (SD); mean selectivity AUC 0.72 ± 0.04) and ipsi (fraction of all cells: 0.14 ± 0.07; mean selectivity AUC 0.31 ± 0.04) whisker stimulation (Figures 3F and S7A). We refer to neurons with significant selectivity as "stimulus-coding" and groups of stimulus-coding neurons in the FOV as ensembles.

Increases in stimulus information in stimulus-coding ensembles were time-locked to stimulus onset (Figures 3G and S8A), and stimulus selectivity was similar irrespective of trial outcome (Figure S8B). Outside of the stimulus presentation window, quantification of whisking did not predict contra vs. ipsi whisker stimulation (Figure S8D bottom), suggesting that active orofacial movements are similar across trial types. Unilateral response amplitude was larger in contra-coding ensembles (preferred-stimulus response (ΔF/F): contra-coding ensembles = 0.18 ± 0.11; ipsi-coding ensembles = 0.12 ± 0.06; ** $p = 0.003$; Wilcoxon signed-rank test; 52 sessions), consistent with an intrahemispheric bias for contralateral input. Across bilateral trials, responses in stimulus-coding ensembles increased as a function of preferred-stimulus intensity (Figures 3G and S7C). Most neurons did not have a statistically significant stimulus preference (fraction of all cells: 0.72 ± 0.09; 183 ± 37.9 cells per FOV; mean AUC 0.5 ± 0.02; Figures 3H and S7B) and did not show reliable responses on average across the stimulus set (Figure 3I). We refer to these neurons as non-coding; however, they could code for variables not explored in the task. Our results therefore indicate that only a sparse subset of L2/3 neurons provide reliable stimulus-coding during task performance.

L2/3 neurons do not predict categorical choice

During imaging sessions, we also included TS trials. As contra-coding ensembles showed stronger responses on bilateral trials, we assessed if contra-coding ensembles predicted choices on TS trials. Average activity patterns were similar on TS trials where mice reported different perceptual choices (Figure 3J top) and different spatial choices (Figure 3J bottom). To quantify this further, we calculated choice probability[24] (CP). CP within stimulus-coding and non-coding ensembles remained at chance across the trial (Figure 3K top and S8E), with no clear correlation between stimulus selectivity and CP across the L2/3 population (Figure S8C top). We also did not find clear evidence of neuronal choice-coding in either symmetric or asymmetric-trained cohorts of mice (Figures S7A and S7D) and did not detect statistically significant choice neurons above the expected false positive rate (5%; Figure S8E). We then calculated a complementary metric we refer to as action probability (AP), with AP scores > 0.5 predicting contralateral lickport choices. Average AP scores also remained at chance (Figures 3K bottom and S8C bottom). We also did not detect significant spatial choice-predictive neurons above chance (Figure S8F).

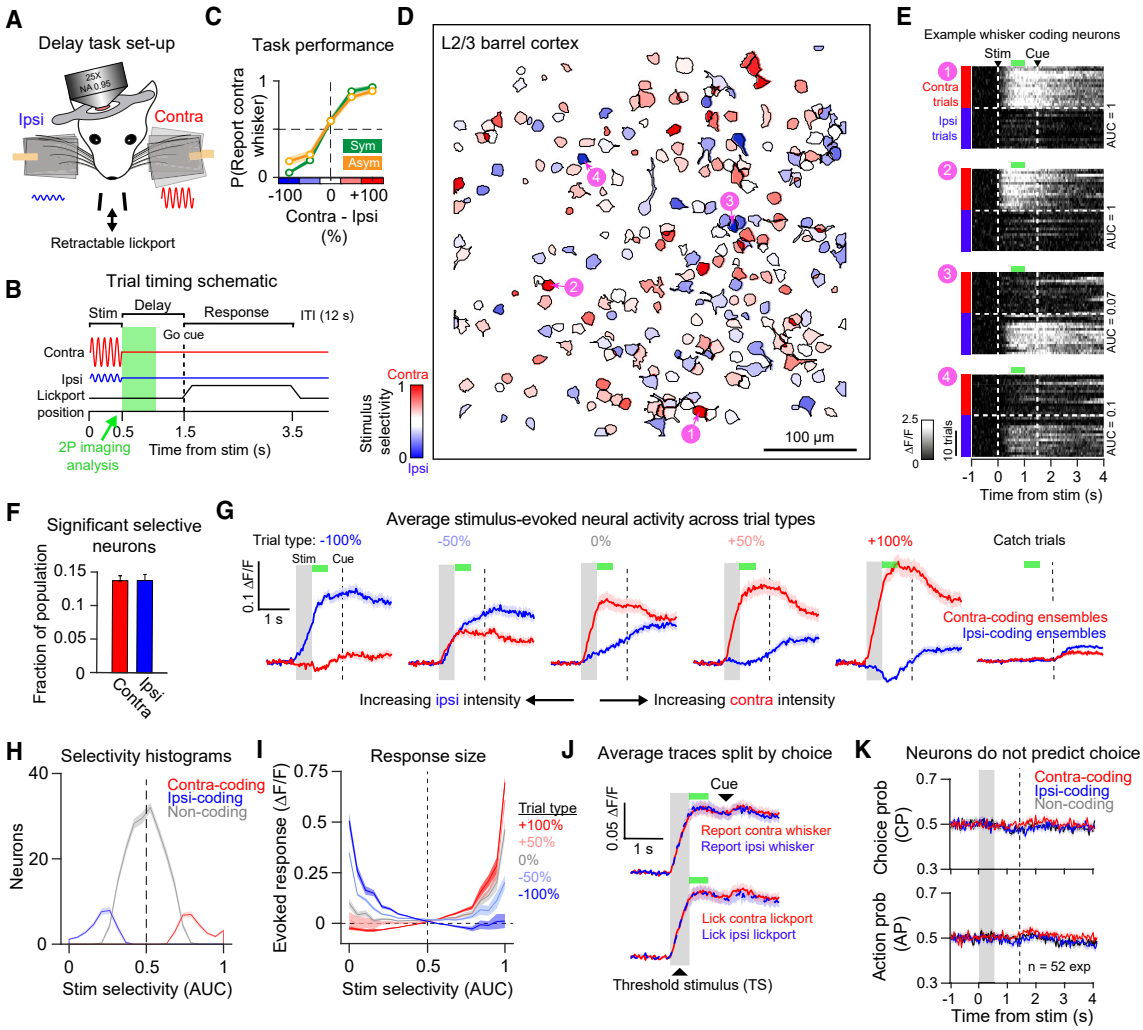

Figure 3. Characterization of task-evoked activity using two-photon calcium imaging

(A) Schematic of the delayed-response discrimination task.

(B) Delay-task trial structure. The green shading denotes the window used to analyze neural activity.

(C) Average psychometric performance during imaging sessions for symmetric (green) and asymmetric (orange) trained mice.

(D) Regions of interest (ROIs) corresponding to neuronal somata in an example FOV colored by stimulus selectivity.

(E) Heat-maps showing sorted single-trial fluorescence responses on unilateral contra (red) and ipsi (blue) whisker trials for 4 example neurons numbered in (D).

(F) Quantification of the mean fraction of significant contra-coding (red) and ipsi-coding (blue) neurons per FOV.

(G) Average trial-evoked fluorescence traces for contra-coding neuron ensembles (red) and ipsi-coding neuronal ensembles (blue) across stimulus trial types in (C).

(H) Histogram showing the average distribution of stimulus-selectivity scores for contra-coding (red), ipsi-coding (blue), and stimulus-non-coding (gray) neurons.

(I) Evoked response amplitude across trial types shown as a function of stimulus selectivity. Colors correspond to different trial types as in (C) and (G).

(J) Average fluorescence traces in contra-coding ensembles on TS trials split by perceptual choice (top) and spatial choice (bottom).

(K) Average choice probability (CP; top) and action probability (AP; bottom) scores in contra (red), ipsi (blue), and non-coding (gray) ensembles across the trial.

Data in Figure 3 are from 52 sessions across 13 mice (30 sessions in 7 symmetric-trained mice; 4.3 ± 2.0 (mean ± SD) sessions per mouse, and 22 sessions in 6 asymmetric-trained mice; 3.7 ± 1.8 (mean ± SD) sessions per mouse). Neural ensemble data were first averaged within session and then presented as the mean ± SEM across sessions.

However, a small proportion of neurons predicted if mice would report a decision vs. miss the trial (proportion of neurons: 0.07 ± 0.04 (mean ± SD); Figure S8G left). We summarized "lick" vs. "no lick" discrimination by calculating detect probability[62] (DP). DP was significantly above chance in stimulus-coding ensembles (DP: contra-coding ensembles; 0.53 ± 0.11; ** p = 0.002; ipsi-coding ensembles 0.52 ± 0.1; ** p = 0.009) but not in non-coding ensembles (DP in non-coding ensembles; 0.5 ± 0.09; n.s. p = 0.32). However, performing the same ROC analysis on videography-extracted movement traces revealed that lick trials could also be predicted from increases in whisking (Figure S8G bottom). Thus, it is possible that neural DP signals are

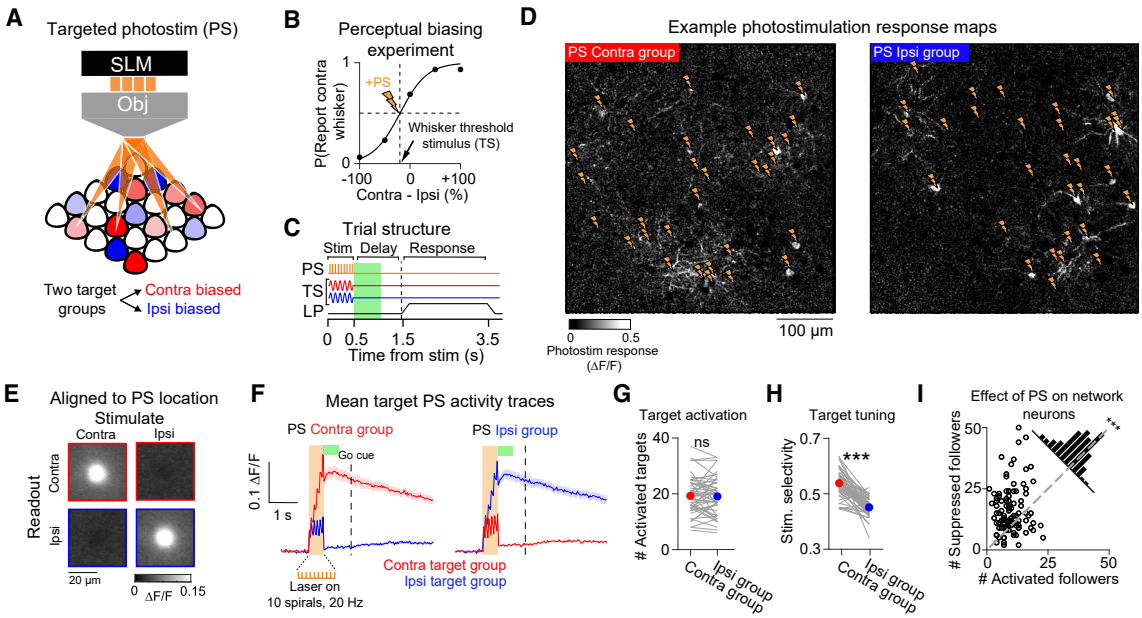

Figure 4. Two-photon photostimulation of L2/3 neurons during whisker discrimination

(A) SLM-targeted two-photon photostimulation (PS) of contra vs. ipsi-biased L2/3 ensembles.

(B) Photostimulation was delivered simultaneously with the whisker threshold stimulus (TS).

(C) Trial structure for paired sensory and photostimulation (TS + PS) trials. The green-shaded region shows the 2P imaging analysis window.

(D) Photostimulation response maps showing the mean response 500–1,000 ms post-stimulus from an example session. Stimulation of the contra and ipsi target groups is shown on the left and right, respectively, with lightning bolts indicating the targeted locations.

(E) Average pixel-wise PS response maps centered on all PS spiral sites for contra (top row) and ipsi (bottom row) SLM targets, on contra group stimulation trials (left column) and ipsi group stimulation trials (right column; average across 1,560 target sites across 52 session).

(F) Average fluorescence traces from contra (red) and ipsi (blue) target neurons on photostimulation trials. The orange bar indicates the photostimulation duration, and the green bar shows the response analysis window. Data are averaged across 52 sets of target groups from 52 sessions across 13 mice; 1,992 activated target neurons in total.

(G) Quantification of the number of target neurons activated by photostimulation during TS + PS trials. The colored marker shows the mean, and gray lines show individual session data.

(H) Same as in (G), but showing quantification of the average stimulus selectivity across activated target groups.

(I) Quantification of the number of suppressed vs. activated network followers during TS + PS trials. 52 sets of followers in 52 sessions; 13 mice; 1,299 activated and 2,078 suppressed follower neurons in total. Statistical comparisons were made across sessions with Wilcoxon signed-rank tests. * $p < 0.05$, ** $p < 0.01$; *** $p < 0.001$.

caused by non-instructed preparatory movements prior to licking. In comparison, whisking did not predict contralateral perceptual choice (Figure S8E bottom) or contralateral lickport choice (Figure S8F bottom). However, lateralized whisking did align with spatial choice during the choice window, consistent with an increase in ipsilateral orofacial movement during directional licking (Figure S8F bottom). Thus, although barrel cortex showed sparse coding of stimulus information, we did not find a consistent predictive relationship between neural responses, or task-evoked movements, and categorical choice.

Targeted 2P PS of L2/3 neurons during behavior

Our experiments in the non-delay task show that manipulating barrel cortex drives lateralized biases in psychophysical performance (Figure 2). However, the number, functional identity, and layer-specificity of neurons "activated" by one-photon optogenetic stimulation are poorly controlled, making it unclear which neurons are involved in driving the behavioral effect. We therefore designed a more powerful all-optical experiment[37,53,54] using 2P targeted PS to test how targeted stimulation of different L2/3 ensembles impacts perceptual choice (Figures 4A–4C). Following task imaging (Figure 3), we selected two groups of 30 pyramidal neurons in the FOV co-expressing GCaMP6s and soma-targeted C1V1 (st-C1V1, Figure S1D) for holographic PS (Figure 4D). We designed target groups with the intention that one would have a contra whisker-selectivity bias, while the other an ipsi bias, by selecting the 30 PS-responsive neurons with the highest and lowest stimulus-selectivity scores, respectively (Figures S9A–S9C). However, as neurons with strong responses to both PS and sensory input were rare (Figures S9D and S9E), this approach likely includes a large number of neurons with weak selectivity. PS was performed using a spatial light modulator (SLM[63–66]; Figure 4A) and a galvanometer-based spiral scanning strategy[53] (STAR Methods). PS-evoked responses were quantified using simultaneous 2P calcium imaging. We paired PS with the whisker TS (TS + PS; Figure 4C) and randomized PS across contra and ipsi-biased target groups across trials.

We parsed neurons into "target" and "network" categories based on lateral somatic proximity to the nearest PS spiral site

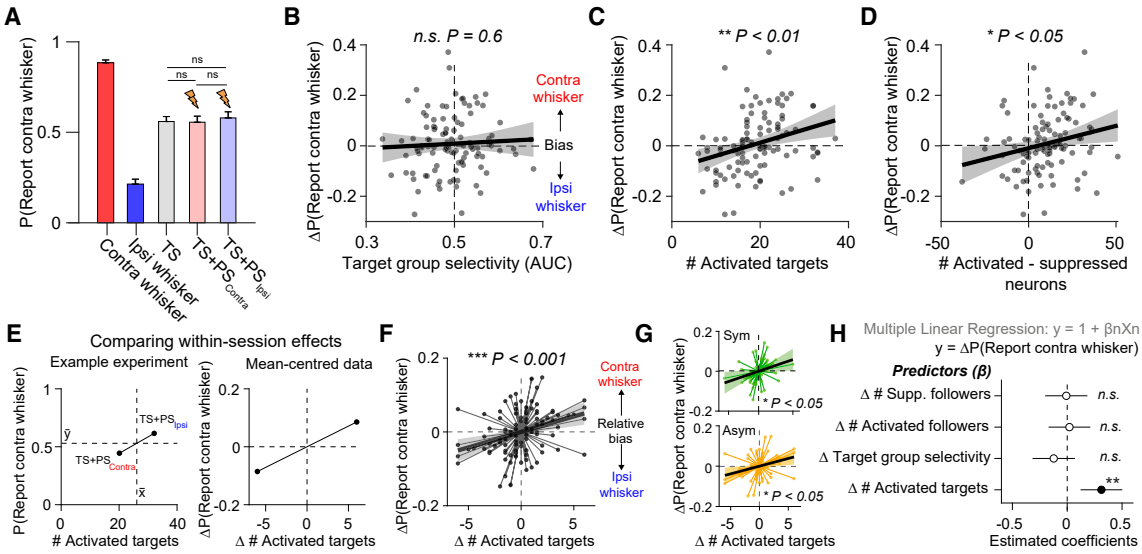

Figure 5. The number of activated target neurons predicts perceptual bias

(A) Quantification of average perceptual choice tendency during the targeted photostimulation experiment.

(B) Comparison of perceptual bias and target group whisker selectivity.

(C) Comparison of perceptual bias and the number of activated target neurons.

(D) Comparison of perceptual bias and the net change in population activity.

(E) Within-session differences across photostimulation conditions were compared by "mean-centering" the data points from each session. This procedure is shown with a single example session. The dashed lines on the left plot indicate the mean P(Report contra whisker) (horizontal) and target response (vertical) across the two conditions.

(F) Correlation between within-session difference in the number of activated targets and perceptual bias across all mean-centered data points. Data points corresponding to the same session are joined with a thin line that passes through the origin.

(G) The same as in (F) but split by sessions from symmetric (green; top) and asymmetric (orange; bottom) trained mice.

(H) A multiple linear regression (MLR) model summarizing the relationship between target and network photostimulation predictors and within-session perceptual bias. Statistically significant predictors are shown with black markers, with error bars indicating 95% coefficient confidence intervals. Data in Figure 5 are from 52 sessions across 13 mice. Each data point represents an individual photostimulation condition (one for TS + PS contra trials and one for TS + PS ipsi trials), with a total of 104 data points. Total number of control TS trials = 2,374, total number of TS trials with PS = 2,403. In correlation plots, shaded error bars denote the 95% confidence bounds of a linear regression fit to the data (black line).

(Figures S10A–S10D). PS evoked soma-shaped increases in fluorescence at the intended spatial locations in the FOV (Figures 4D and 4E) and stimulation-locked fluorescence increases in the corresponding target groups (Figure 4F). We refer to neurons in target "zones" with significant activity increases on PS trials as activated targets. Although we targeted 30 neurons in each experiment, not all of them responded with significant increases in activity (# activated targets in TS + PS contra group 19.3 ± 6.5; mean ± SD; # activated targets in TS + PS ipsi group = 19.1 ± 6.8; n.s. p = 0.72; Wilcoxon signed-rank test; n = 52 sessions; Figure 4G). The number of activated targets on PS and TS + PS trials was highly correlated (Figure S10E) and was also correlated with the number of PS-responsive neurons in the FOV, as expected (Figure S10F). The number of activated targets was also closely related to the total number of neurons located within target zones' (Figure S10G), which we did not control for experimentally. The activated target groups had a weak, but consistent, whisker stimulus-selectivity bias (mean selectivity difference across groups = 0.083 ± 0.063, $p = 5.3 \times 10^{-9}$; Figure 4H). We also quantified the impact of targeted PS on non-targeted "follower" network neurons. Across experiments, we found that a larger number of followers were suppressed on TS + PS trials (# activated followers: 12.5 ± 5.6; # suppressed followers: 20 ± 11.5; *** $p = 8.9 \times 10^{-8}$; Wilcoxon signed-rank test; n = 104 PS conditions; 52 sessions; Figure 4I). Thus, patterned 2P PS resulted in the activation of neurons within target zones while predominantly suppressing neurons in the local L2/3 network.

Perceptual bias scales with the number of photostimulated L2/3 neurons

PS of small ensembles did not result in average changes in choice tendency on TS trials (P[Report contra whisker] on TS trials: 0.56 ± 0.2; 45.7 ± 21.7 trials; mean ± SD; on TS + PS contra trials: 0.56 ± 0.24; 22.8 ± 10.5 trials; n.s. p = 0.68; on TS + PS ipsi trials: 0.58 ± 0.24; 23.4 ± 10.8 trials; n.s. p = 0.33; Wilcoxon signed-rank test; n = 52 sessions; Figure 5A). Across sessions, target group whisker selectivity also did not predict perceptual bias (Pearson's corr (r) = 0.05; n.s. p = 0.06; Figure 5B). Instead, we found that perceptual bias significantly correlated with the number of activated target neurons (Pearson's corr (r) = 0.3; ** p = 0.002; Figure 5C). This correlation was maintained when using different statistical thresholds for defining activated targets (Figure S11A) and was absent when we repeated our analysis on resampled control TS trials (Figure S11B). Moreover, target

groups did not show CP on control trials that differed from chance (Figure S11C), and target group CP did not predict the impact of PS on behavior or the number of activated targets across sessions (Figure S11D).

Intriguingly, activating low numbers of targets appeared to bias choice toward the ipsilateral whisker (Figure 5C). By quantifying the number of activated vs. suppressed neurons across both targets and followers, we found that perceptual bias also correlated with net change in population activity (Pearson's corr (r) = 0.23; * p = 0.02; Figure 5D). This suggests that ipsilateral biases tended to occur in sessions where PS was comparatively weak, and thus the net effect on the L2/3 circuit was slightly suppressive (Figure 5D). However, quantification of follower neurons alone was not sufficient to predict changes in behavior (Figure S11E), suggesting that the impact of PS on perceptual bias cannot be wholly explained by differences in network state.

Within-session perceptual bias correlates with the number of activated target neurons

As we stimulated two target groups per session, we then analyzed whether differences in the number of activated target neurons explained variability in within-session perceptual bias. To examine this effect, we mean-centered the data points from the two PS conditions from each session (Figure 5E). Across the mean-centered dataset, variability in the number of activated targets also significantly correlated with relative perceptual bias (Pearson's corr (r) = 0.33; *** p = 0.0007; Figure 5F). This correlation was present in both symmetric (Pearson's corr (r) = 0.33; * p = 0.011; n = 30 sessions, 7 mice; Figure 5G Top) and asymmetric-trained cohorts of mice (Pearson's corr (r) = 0.34; * p = 0.025; n = 22 sessions, 6 mice; Figure 5G bottom). We used a multiple linear regression model to summarize within-session effects of PS on perceptual choice bias (Figure 5H). Perceptual bias was significantly predicted by the number of activated targets (estimated coefficient = 0.31; t-stat = 3.3; ** p = 0.001) but not the number of activated (estimated coefficient = 0.03; t-stat = 0.32; n.s. p = 0.74) or suppressed (estimated coefficient = −0.01; t-stat = −0.5; n.s. p = 0.96) follower neurons. Perceptual bias was also not correlated with target group whisker stimulus selectivity (estimated coefficient = −0.16; t-stat = −1.6; n.s. p = 0.1). Additional analysis confirmed that neither perceptual bias nor the number of activated target neurons correlated with differences in pre-stimulus network fluorescence or peri-stimulus whisking or body movement across PS trial types (Figure S11F). Thus, our results indicate that sparse unilateral manipulation of the L2/3 circuit during bilateral discrimination causally drives a lateralized perceptual bias that scales with the number of neurons activated.

Activation of task-silent target neurons predicts perceptual bias

Our findings indicate that the perceptual effect of L2/3 PS during our task is predicted by the number, and not tuning, of activated target neurons (Figures 5B and 5H). However, although the target groups did show an average stimulus-selectivity bias (Figure 4H), additional analysis revealed that the majority of activated targets did not have a statistically significant whisker stimulus preference (Figure 6A). As stimulation predominantly activated non-coding target neurons in the circuit, we assessed whether this was sufficient to predict the perceptual effect of targeted PS. A multiple linear regression analysis (Figure 6B) confirmed that the number of activated non-coding target neurons significantly predicted perceptual bias (estimated coefficient = 0.3; t-stat = 3.14; ** p = 0.002). In comparison, neither the number of activated contra-coding targets (estimated coefficient = 0.05; t-stat = 0.46; n.s. p = 0.64) nor the number of ipsi-coding targets (estimated coefficient = 0.03; t-stat = 0.32; n.s. p = 0.75) predicted the behavioral effect. The correlation between non-coding target neuron activation and perceptual bias was present across sessions (Pearson's corr (r) = 0.31; ** p = 0.001; Figure S12A) and within a session (Pearson's corr (r) = 0.21; * p = 0.03; Figure S12B).

Non-coding target neurons showed reliable PS-evoked responses but did not show whisker-evoked activity (Figure 6C). This was consistent for non-coding target neurons in the contra-biased and the ipsi-biased target groups (Figure S13). Analysis of behavioral videography also revealed that trials with whisker stimulation evoked sustained increases in active whisking, body movement, and licking (Figures 6D and S6C). As fluorescence in non-coding target neurons remained at pre-stimulus levels throughout the trial epoch, this indicates that the non-coding target neurons are also not significantly activated by task-evoked movements. Our findings therefore indicate that small numbers of "task-silent" L2/3 neurons, which show no clear functional relationship to sensory, motor, or reward variables during task performance, can influence perceptual decisions if recruited into the active population through targeted optogenetic manipulation.

Patterned stimulation reveals the specificity of L2/3 inhibition during whisker processing

Comparing target responses across trial types revealed that PS responses were notably larger in the absence of concurrent whisker stimulation, particularly in ipsi-coding and non-coding target neurons (Figure 6C). This prompted us to examine the interaction between sensory and PS-triggered activity patterns (Figure 7A). For some targets, PS responses were near abolished on TS + PS trials, and all PS target locations showed a reduction in fluorescence when comparing PS trials with TS + PS trials (Figure 7B). To assess the relationship between the decrease in PS response and the TS-evoked sensory response, we quantified the average difference in the target group response on PS and TS + PS trials and compared this with the average response to TS input in the TS-responsive non-targeted network neurons (Figure 7C). Across sessions, the change in target group PS response was negatively correlated with the network response to sensory input (Pearson's corr (r) = −0.49; *** $p = 1.3 \times 10^{-7}$; Figure 7D). This indicates that the stronger the whisker-evoked response in the network, the stronger the suppressive effect on PS-evoked activity in the target neurons.

To examine whether this effect showed specificity at the single neuron level, we quantified fluorescence responses across trial types in all activated targets as a function of whisker responsiveness (Figure 7E). We defined whisker responsiveness as the AUC score from an ROC analysis comparing TS with catch trial responses and adjusted scores between −1 and 1 such that the

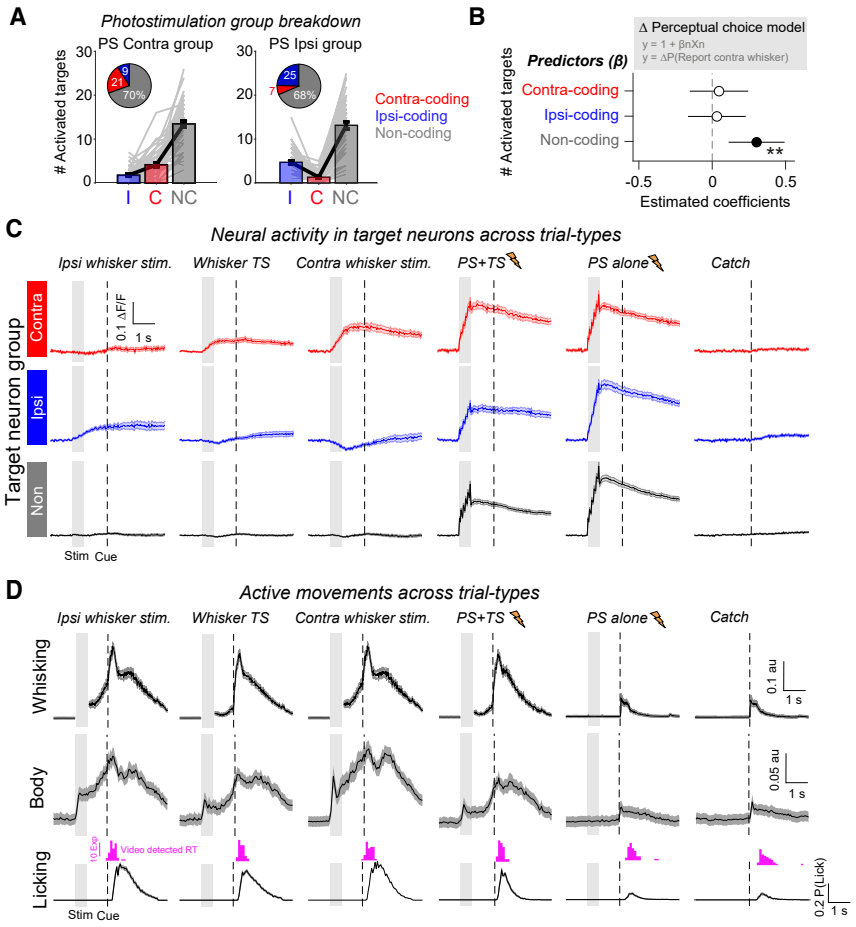

Figure 6. Photostimulation of non-coding neurons predicts perceptual bias

(A) Quantification of the number of contra-coding (red), ipsi-coding (blue), and whisker non-coding (gray) activated target neurons that made up the two photostimulation target groups. Individual lines show individual sessions. The inset circle charts indicate the average proportional group summary.

(B) A multiple linear regression (MLR) model summarized the relationship between the number of photostimulated stimulus-coding and non-coding neurons and perceptual bias. Marker points shown the estimated coefficients with error bars indicating the 95% confidence intervals.

(C) Trial-evoked activity traces from contra-coding (red), ipsi-coding (blue), and non-coding (gray) photostimulation target neurons are shown across different trial types.

(D) The time course of average trial-evoked contralateral whisking (top), body movement (middle), and licking (bottom) behavioral measures are shown across trial types. The magenta histogram shows the distribution of mean reaction times assessed using videography. Note that during whisker stimulation (gray shading), we do not plot whisking traces as it is unclear which whisker movements are driven by the stimulus and which are the result of active movement. Data in Figure 6 are from 52 sessions in 13 mice. Total number of neurons analyzed: 274 contra-coding targets; 329 ipsi-coding targets; and 1,381 non-coding targets. Data are shown as the mean and SEM across sessions.

sign denoted negative vs. positive modulation by TS input. We then calculated the difference between measured TS + PS responses and the expected linear sum of separate TS and PS trial-evoked responses as an approximation for sensory-induced suppression of PS activity (Figure 7F). Target neurons with high whisker responsiveness scores appeared largely unaffected by sensory-induced network suppression. By contrast, neurons with lower whisker responsiveness scores and those with negative scores showed a large difference. When quantifying this effect with respect to stimulus-coding groups, we found that contra-coding targets groups showed no difference between measured and expected response (0.004 ± 0.01; n.s. p = 0.78), whereas both ipsi-coding target groups (−0.11 ± 0.11; *** $p = 2.6 \times 10^{-8}$) and non-coding target groups (−0.1 ± 0.07; *** $p = 6.3 \times 10^{-10}$) showed a strong suppression of PS activity on TS trials (Figure 7F *inset*). Thus, patterned PS revealed recruitment of potent cortical inhibition in L2/3 during whisker processing that appeared to preferentially impact ipsi-coding and non-coding neurons in the L2/3 circuit.

Patterned stimulation suppresses local whisker-evoked signals

We next investigated the impact of patterned PS on whisker-evoked responses in the local circuit by analyzing TS-responsive neurons that were not targeted for PS. On average, targeted PS reduced the amplitude of the TS-response in network neurons (ΔTS response = −0.02 ± 0.015 ΔF/F; *** $p = 9.7 \times 10^{-18}$, −19.4 ± 13.6% proportional change; n = 104 PS conditions, 52 sessions). This reduction was correlated with the amplitude of PS response in the target groups (Pearson's corr (r) = −0.21; * $p = 0.04$; Figure 7G). The magnitude of sensory response suppression was stronger for network neurons in close proximity to large numbers of PS-activated target neurons (Figure 7H), suggesting that the suppressive effect of PS on the local circuit decreases with distance. All non-targeted TS-responsive neurons showed reduced TS responses on TS + PS trials on average (Figure 7I), with those that were part of contra-coding ensembles tending to show larger absolute changes in ΔF/F (Figure 7I *inset*). However, neurons with larger whisker responsiveness scores showed smaller proportional changes relative to the baseline amplitude of the TS-evoked response (Figure 7J). As strongly whisker-responsive neurons were relatively less inhibited by network-evoked suppression, this indicates that global inhibition may serve an important role in selectively eliminating weak responses in the circuit.

Competitive interactions between contralateral and ipsilateral whisker signals in L2/3

Finally, we performed additional experiments to examine interactions between contra and ipsi-evoked signals in L2/3. After the targeted PS experiment, we mapped passive neuronal

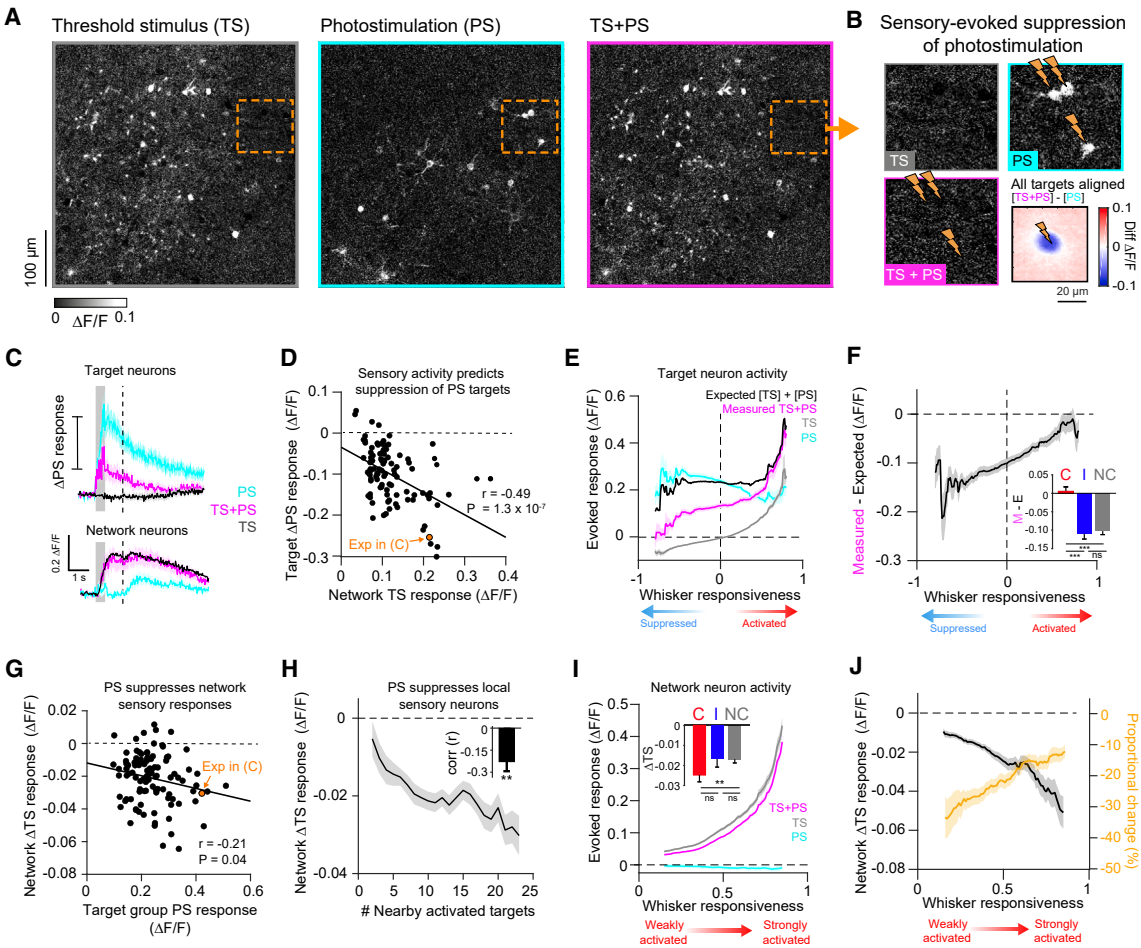

Figure 7. Patterned photostimulation reveals potent inhibitory pressure in L2/3 during task performance

(A) Response maps for threshold stimulus (TS; gray), photostimulation (PS; cyan), and combined TS and PS (magenta) trials for an example session.

(B) Close up of the orange-bounded region shown in (A). Lightning bolts indicate the location of PS targets. Bottom right shows the average pixel-wise fluorescence difference across TS + PS and PS trials center-aligned on all photostimulation target locations.

(C) Extracted fluorescence traces from target neurons (top; $n = 23$ neurons) and TS-responsive network neurons (bottom; $n = 57$ neurons) across trial types from the example session in (A).

(D) Suppression of photostimulation responses in the target neuron group on PS vs. TS + PS trials is correlated with the mean response to TS whisker trials in non-targeted network cell group. Each data point represents a single photostimulation condition.

(E) Responses in photostimulation target neurons across different trial types are plotted as a function of whisker responsiveness.

(F) The difference between the measured (magenta in E) and expected (black in E) response to combined TS and PS stimuli in target neurons is plotted as function of whisker responsiveness. The inset shows quantification of this difference averaged across contra-coding (red), ipsi-coding (blue), and non-coding (gray) target neuron ensembles.

(G) Suppression of TS responses in network neuron groups on TS + PS trials is plotted against average PS-evoked responses in target neuron groups.

(H) Average PS-evoked suppression of TS responses in network neurons is binned as a function of the number of nearby activated target neurons (counted within a 200 µm radius). The inset shows the average Pearson's correlation coefficient between sensory suppression and number of nearby targets across sessions ($r = -0.21 \pm 0.47$; mean ± SD; ** $p = 0.002$ Wilcoxon signed-rank test tested against 0).

(I) Responses in TS-responsive network neurons across trial types are plotted as a function of whisker responsiveness. The inset shows quantification of the change across TS and TS + PS trials with respect to ensemble groups as in (F).

(J) The difference in network neuron response on TS and TS + PS is shown as a function of whisker responsiveness. The absolute change is shown in black, and the proportional change relative to TS baseline is shown in orange. Data in Figure 7 come from 104 photostimulation conditions across 52 sessions in 13 mice. Total number of target neurons analyzed = 1,992; total number of network neurons analyzed = 2,429. Total number of trials analyzed: 3,466 TS, 3,568 PS; 3,447 TS + PS trials. Data are shown as the mean and SEM across sessions. Statistical comparisons were Wilcoxon signed-rank test. n.s. $p > 0.05$; * $p < 0.05$; ** $p < 0.01$; *** $p < 0.001$.

responses to a "3 × 3" stimulus set of unilateral and bilateral stimuli (Figures 8A and 8B). Contra-coding ensembles, defined based on activity during the behavioral experiment, showed large responses to contralateral stimulation that appeared robust to concurrent ipsilateral whisker stimulation (Figure 8B top). By contrast, ipsilateral-evoked signals in ipsi-coding

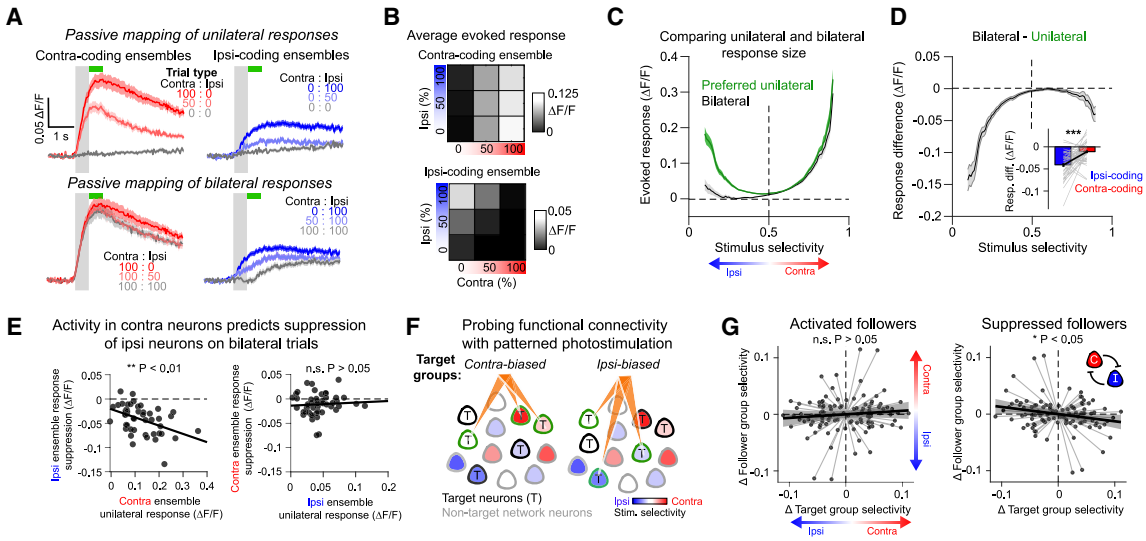

Figure 8. Antagonistic interactions between contra and ipsi-coding neurons in L2/3

(A) Fluorescence traces in contra-coding (left; red) and ipsi-coding (right; blue) ensembles across unilateral (top) and bilateral (bottom) whisker deflection intensities (%).

(B) Quantification of the mean fluorescence responses across a 3 × 3 matrix stimulus set in contra-coding (top) and ipsi-coding (bottom) ensembles (average ensemble response across 52 sessions).

(C) Comparison of responses to preferred unilateral whisker stimulation (green; 100% unilateral stimulation) and matched bilateral whisker stimulation (black; 100% bilateral stimulation) plotted as a function of stimulus selectivity.

(D) The difference in unilateral and bilateral responses (shown in C) is plotted as a function of stimulus selectivity. The inset shows quantification of this difference in contra and ipsi-coding ensembles (n = 52 sessions; Wilcoxon signed-rank test; *** $p < 0.001$; thin gray lines show individual sessions).

(E) Comparison of response suppression in one ensemble group on bilateral trials with the unilateral response in the other ensemble group. Each marker point represents an individual session, 52 sessions in total. Total number of contra-coding neurons analyzed 1,907; ipsi-coding neurons 1,925.

(F) Probing functional connectivity in the circuit using targeted photostimulation of whisker-biased target groups.

(G) Comparing average whisker selectivity of network followers in response to targeted photostimulation. Correlations are measured across 104 mean-centered data points (2 photostimulation conditions per session, 52 sessions in total). Shaded error bars denote the 95% confidence bounds of a linear regression fit to the data.

ensembles were weaker and appeared strongly suppressed by concurrent contralateral stimuli (Figure 8B bottom). We compared responses to the preferred unilateral stimulus (100% intensity) to bilateral stimulation (100% intensity on both sides) as a function of stimulus selectivity (Figure 8C) and calculated the difference between the bilateral and preferred unilateral response (Figure 8D). Contra-coding ensembles showed a modest reduction in response on bilateral stimulation trials (change in response (ΔF/F): −0.01 ± 0.02; ** $p = 0.001$; Wilcoxon signed-rank test; n = 52 sessions), whereas ipsi-coding ensembles showed stronger attenuation (change in response (ΔF/F): −0.04 ± 0.03; *** $p = 3.7 \times 10^{-9}$; Figure 8D *inset*). The difference between contra and ipsi-coding ensemble suppression was significant (*** $p = 1.9 \times 10^{-5}$).

Across sessions, bilateral suppression of the ipsilateral ensemble was correlated with the contra-coding ensemble response to unilateral contralateral stimulation (Pearson's corr (r) −0.44; ** $p = 0.002$; Figure 8E left). The inverse relationship between contra-coding ensemble suppression and the ipsi-coding ensemble response was not significant (Pearson's corr (r) 0.07; n.s. $p = 0.66$; Figure 8E right). This indicates that contra-evoked signals may dominate during bilateral whisker processing by suppressing ipsi-responses in the circuit. To directly examine this relationship, we performed additional analysis of our PS dataset to assess whether the whisker selectivity of the PS target groups correlated with the selectivity of recruited follower neurons. For each session, we restricted our analysis to neurons that were not part of either activated target group, and thus, we could directly compare the local circuit response to two different photostimuli (Figure 8F). Across the dataset, variability in target group whisker selectivity did not correlate with variability in the average whisker selectivity of the activated followers (Pearson's corr (r) = 0.1; n.s. $p = 0.32$; Figure 8G left). However, target group whisker selectivity negatively correlated with the selectivity of the suppressed followers (Pearson's corr (r) = −0.23; * $p = 0.018$; Figure 8G right), indicating that stimulation of L2/3 contra-coding neurons tends to suppress ipsi-coding neurons in the FOV and vice versa. Thus, our findings demonstrate that strong competitive interactions between different L2/3 ensembles dominate sparse cortical dynamics and provide evidence that mutual inhibition between contra and ipsi-coding ensembles may be a prominent feature of intrahemispheric L2/3 activity during cross-hemispheric sensory processing.

DISCUSSION

We combined 2P calcium imaging and 2P PS to probe sparse coding in the barrel cortex during a challenging discrimination

task. We show that sparse coding of whisker stimuli is ensured by preferential sensory-evoked inhibitory suppression of non-coding neurons, which helps to ensure a high signal-to-noise ratio for the detection of small perturbations. Moreover, although contralateral and ipsilateral whisker signals were represented in sparse subsets of stimulus-coding L2/3 neurons during task performance, the effect of intrahemispheric PS on lateralized perceptual bias depended on the number of non-coding target neurons activated. This suggests that non-coding neurons can be engaged to enhance sensory processing, which could be achieved endogenously via neuromodulation[67,68] or cortical plasticity.[22,49]

A whisker discrimination task to probe tactile perception

We developed a behavioral task framework suitable for probing the link between neural circuit activity in sensory cortex and behavior.[69] Through both gain- and loss-of-function perturbations, we demonstrate that the perceived intensity of contralateral whisker input is causally linked to barrel cortex activity. By manipulating the bilateral stimulus interval in the non-delay task, we also found that unilateral percepts were formed rapidly and showed robustness to late-arriving distraction characteristic of choice-related attractor state dynamics.[70] The barrel cortex-dependent sensory integration window, which we estimate to be ~100 ms based on temporal discrimination and photoinhibition experiments, is comparable to cortical processing windows in other whisker tasks[26,71,72] and tasks using other sensory modalities.[73] It is also consistent with findings showing that whisker input and microstimulation-induced activity quickly spread from barrel cortex to high-order sensory and motor areas,[74,75] and demonstrates that barrel cortex plays a causal role in initiating rapid sensorimotor transformations during goal-directed behavior. Despite coding stimulus information, we did not find choice signals in barrel cortex. However, choice could be represented in membrane potential dynamics[26] or temporal spike patterns,[76] which may be difficult to resolve using calcium imaging, or in deeper cortical layers, which we did not sample during our experiments. Alternatively, decision-related processing may occur downstream from S1 in areas that also integrate bilateral whisker input, such as striatum[77] and/or S2.[78,79] Future work is required to investigate the downstream circuits implicated in the decision process to further elucidate the role of barrel cortex in coordinating cross-hemispheric perceptual behavior.

Interhemispheric processing in the barrel cortex

Cross-hemispheric projections are a prominent feature of many cortical circuits.[80–83] Surprisingly, we find that L2/3 contains equal proportions of ipsilateral and contralateral whisker-selective neurons, and also that strong competitive interactions between bilateral tactile signals occur at the level of primary somatosensory cortex during perceptual decision-making. This extends previous work characterizing bilateral responses in barrel cortex, which has predominantly been performed under anesthesia or in non-behaving states.[79,84,85] Although ipsilaterally tuned neurons showed robust activity on unilateral trials, they were strongly attenuated by concurrent contralateral whisker stimulation. These findings support previous evidence that the short cross-callosal latency makes ipsilateral signals susceptible to rapid feedforward recruitment of cortical inhibition by contralateral-evoked thalamocortical input during bilateral stimulation,[84–88] further indicating that the integration of bilateral tactile signals may relate to the precise spatiotemporal sequence of whisker stimulation.[84,85]

Our behavioral experiments also indicate that competition between hemispheres plays an important role in task-related perceptual processing. For example, results from the one-photon optogenetic-biasing experiments (Figure 2I) show that manipulating one hemisphere has an equal but opposite effect on the reaction time for the non-stimulated hemisphere. The push-pull direction of this bias switches depending on whether one delivers unilateral photoinhibition or photoactivation, providing strong causal evidence that both hemispheres have the capacity to directly compete during whisker-guided behavior.[89–92] In rodent cortex, several mechanisms can mediate inhibitory interactions between hemispheres. These include transcallosal feedforward recruitment of local PV interneurons,[79,83,92,93] recruitment of interneurons in superficial layers, which subsequently inhibit the distal dendrites of neurons in deeper layers,[91] as well as via long-range callosally projecting inhibitory neurons.[93] The extent to which these different inhibitory pathways are engaged in parallel or differentially under stimulus-specific or task-specific conditions remains unclear. Moreover, callosal interactions also mediate more refined functions, including the homotopic transfer of sensorimotor signals and learned information,[82,94,95] and shaping receptive fields and circuit plasticity.[89,90,96] Future work is therefore needed to elucidate how organization of callosal microcircuits shapes bilateral somatosensation.

Intracortical inhibition enforces sparse coding in L2/3

Our experiments revealed strong antagonism between contralateral and ipsilateral-selective neurons, as well as competition between PS and sensory-evoked signals in L2/3. This demonstrates that recruitment of inhibition is the basis of competitive interactions between different cortical excitatory ensembles during awake behaving states[16,17,97] and highlights the utility of combining patterned optogenetic stimulation and population calcium imaging to probe functional dynamics in neural circuits.[98–101] PS responses were strikingly attenuated when paired with simultaneous whisker deflection. This suggests that strong inhibitory mechanisms are engaged during task performance to balance network excitation, which under our task conditions could accumulate across feedforward,[14,15,86,87,102] feedback,[103] lateral,[104,105] and inter-hemispheric[91] sources. In line with other recent studies, we also found that targeted stimulation of pyramidal neurons suppressed other non-targeted pyramidal neurons in the local L2/3 circuit.[37,98,105,106] This provides further evidence that dense connectivity between excitatory and inhibitory neurons mediates strong lateral competition in cortex[10,88,105–107] and that the recruitment of local inhibitory mechanisms scales with the number of concurrently activated pyramidal neurons.[37,97,104]

More generally, our results not only indicate that strong inhibitory pressure plays a major role in enforcing the sparsity of cortical responses,[16,88,97] but that inhibition is selective.

PS-evoked suppression of network neurons had the greatest proportional effects on responses that were initially small, consistent with previous findings indicating that disproportionate effects of cortical inhibition across heterogenous populations of barrel cortex neurons may serve to enhance sparse whisker coding.[104,108] This suggests that interactions between excitatory and inhibitory microcircuits exhibit a specific structure to enhance the signal-to-noise ratio of robust sensory signaling while maintaining sparsity of responses.

Small numbers of non-coding neurons can contribute to perception

Using all-optical interrogation, we demonstrate that targeted manipulation of surprisingly few L2/3 neurons can result in measurable biases in whisker-guided choices. This is consistent with recent barrel cortex studies showing that stimulation of small neural ensembles[37,109] (and even single neurons[35,42]) can evoke perceptual effects. Surprisingly, we found that perceptual bias was significantly predicted by the number of non-coding neurons activated by targeted PS, challenging the consensus that decision-making processes read out activity from highly tuned stimulus-responsive neurons.[110] Non-coding neurons did not show stimulus, movement, or reward-related activity, which is intriguing as recent studies have demonstrated that non-instructed movements can profoundly influence the activity of cortical neurons.[111,112]

In contrast with recent studies involving the selective optical stimulation of functionally tuned neurons during behavior,[43,45,46,100,109,113,114] we did not find a significant effect of target ensemble tuning on task performance. One factor may be that in our experiments, target group whisker selectivity was relatively weak as we predominantly stimulated non-coding neurons (in particular because finding neurons with strong responses to both whisker input and 2P stimulation in the FOV was rare). In the future, this could be resolved by interrogating larger[99] and/or volumetric FOVs[46,115] to provide a larger sample of strongly tuned neurons. Thus, although further work is needed to investigate the differential contributions of contra- and ipsi-coding neurons to bilateral somatosensation, we provide compelling evidence that stimulus-non-coding neurons can be recruited to enhance sensory perception.

It remains to be established whether stimulus-non-coding neurons can influence performance in other perceptual contexts. Recent work in visual cortex suggests that stimulating non-coding neurons can even impair performance by suppressing the perceptually relevant cells in the local circuit,[45] suggesting that the ability of non-coding neurons to influence perception may depend on task design or brain area. In our experiments, the dynamics of interhemispheric competition might engage a distinct decision-making process that prioritizes rapid decoding of intrahemispheric spiking across a wider pool of neurons in barrel cortex in a winner-take-all scenario. Under perceptually ambiguous conditions, any additional intrahemispheric spikes may thus help reach a decision threshold, which could also reflect increased capacity for the photostimulated hemisphere to suppress the contralateral hemisphere,[84,85] compensate for cortical adaptation to high-frequency whisker stimulation[116] or enhance sensory responses in deeper cortical layers.[117,118]

A reserve pool of silent neurons can be recruited to influence behavior

The observation of large fractions of stimulus-non-responsive neurons in cortex has long been intriguing.[23,47,48] These "silent" neurons could be suppressed by intrinsic or synaptic mechanisms to constrain excessive cortical excitation, reduce coding redundancy, and/or increase energy efficiency via sparse coding.[50,119–121] Our results suggest that under our task conditions, non-coding neurons are able to influence task performance but are normally suppressed by strong network inhibition during task-related whisker processing. Releasing these neurons from inhibitory suppression, as we achieved through patterned optogenetic stimulation but which could be achieved endogenously via disinhibitory VIP+ interneuron circuits[122] and cortical plasticity,[22,49] may therefore provide a simple mechanism for enhancing intracortical sensory signals in some contexts. Our findings also add causal support to emerging evidence showing that neurons in sensory cortex without stimulus-driven responses can contribute to neural processing.[123–127] These results have important implications for designing novel therapeutic optical brain-machine interfaces and optogenetic therapies,[128] since they suggest that it may not be necessary to precisely target optogenetic interventions to specific functionally defined pools of neurons. Rather, activation of a relatively small pool of pyramidal neurons regardless of functional identity could be sufficient to enhance sensory coding and restore some basic sensorimotor functions.

STAR★METHODS

Detailed methods are provided in the online version of this paper and include the following:

- KEY RESOURCES TABLE
- RESOURCE AVAILABILITY
  - Lead contact
  - Materials availability
  - Data and code availability
- EXPERIMENTAL MODEL AND PARTICIPANT DETAILS
- METHOD DETAILS
  - Surgical procedures
  - Whisker stimulation
  - Behavioral training
  - Behavioral metrics
  - Behavioral videography
  - Muscimol silencing
  - Widefield calcium imaging
  - One-photon optogenetics
  - All-optical system design
  - Photostimulation response mapping
  - Two-photon calcium imaging data
  - Identifying neurons with significant trial responses
  - Pixel-wise analysis of imaging data
  - Receiver operating characteristic analysis
  - Control trial resampling
- QUANTIFICATION AND STATISTICAL ANALYSIS
  - Statistical analyses

SUPPLEMENTAL INFORMATION

Supplemental information can be found online at https://doi.org/10.1016/j.neuron.2024.04.015.

ACKNOWLEDGMENTS

We thank Selmaan Chettih and Christopher Harvey for developing and sharing the somatically restricted C1V1 opsin, Soyon Chun for mouse breeding, members of the UCL Biological Service Unit for animal care and husbandry, Hamish Forrest for behavioral training during pilot experiments, and Bruker Corporation for technical support. We also thank Ann Duan, Sonja Hofer, and Miguel Maravall for useful discussions. This work was supported by grants from the Wellcome Trust (PRF 201225 and 224688), the ERC (AdG 695709), the MRC (MR/T022922/1), and the BBSRC (BB/N009835/1).

AUTHOR CONTRIBUTIONS

O.M.G. conducted 2P imaging and photostimulation experiments with input from L.E.R., A.M.P., H.W.P.D., and M.H. O.M.G., M.I., and F.S. conducted behavioral training and 1P optogenetic experiments. O.M.G. and M.I. analyzed videography data. L.E.R. developed behavioral training software. A.M.P., L.E.R., and H.W.P.D. designed and built the all-optical microscope used for experiments. L.E.R. and H.W.P.D. developed software for photostimulation control. O.M.G. performed surgeries. O.M.G. analyzed data with input from all authors. O.M.G. and M.H. wrote the manuscript with input from all authors.

DECLARATION OF INTERESTS

The authors declare no competing interests.

Received: July 31, 2023
Revised: February 12, 2024
Accepted: April 12, 2024
Published: May 9, 2024

REFERENCES

1. O'Connor, D.H., Huber, D., and Svoboda, K. (2009). Reverse engineering the mouse brain. Nature *461*, 923–929. https://doi.org/10.1038/nature08539.
2. Panzeri, S., Harvey, C.D., Piasini, E., Latham, P.E., and Fellin, T. (2017). Cracking the Neural Code for Sensory Perception by Combining Statistics, Intervention, and Behavior. Neuron *93*, 491–507. https://doi.org/10.1016/j.neuron.2016.12.036.
3. Ohki, K., Chung, S., Ch'ng, Y.H., Kara, P., and Reid, R.C. (2005). Functional imaging with cellular resolution reveals precise micro-architecture in visual cortex. Nature *433*, 597–603. https://doi.org/10.1038/nature03274.
4. Lefort, S., Tomm, C., Floyd Sarria, J.C., and Petersen, C.C.H. (2009). The Excitatory Neuronal Network of the C2 Barrel Column in Mouse Primary Somatosensory Cortex. Neuron *61*, 301–316. https://doi.org/10.1016/j.neuron.2008.12.020.
5. Cossell, L., Iacaruso, M.F., Muir, D.R., Houlton, R., Sader, E.N., Ko, H., Hofer, S.B., and Mrsic-Flogel, T.D. (2015). Functional organization of excitatory synaptic strength in primary visual cortex. Nature *518*, 399–403. https://doi.org/10.1038/nature14182.
6. Peron, S., Pancholi, R., Voelcker, B., Wittenbach, J.D., Ólafsdóttir, H.F., Freeman, J., and Svoboda, K. (2020). Recurrent interactions in local cortical circuits. Nature *579*, 256–259. https://doi.org/10.1038/s41586-020-2062-x.
7. Ko, H., Hofer, S.B., Pichler, B., Buchanan, K.A., Sjöström, P.J., and Mrsic-Flogel, T.D. (2011). Functional specificity of local synaptic connections in neocortical networks. Nature *473*, 87–91. https://doi.org/10.1038/nature09880.
8. Harris, K.D., and Mrsic-Flogel, T.D. (2013). Cortical connectivity and sensory coding. Nature *503*, 51–58. https://doi.org/10.1038/nature12654.
9. Brecht, M., Roth, A., and Sakmann, B. (2003). Dynamic receptive fields of reconstructed pyramidal cells in layers 3 and 2 of rat somatosensory barrel cortex. J. Physiol. *553*, 243–265. https://doi.org/10.1113/jphysiol.2003.044222.
10. Packer, A.M., and Yuste, R. (2011). Dense, Unspecific Connectivity of Neocortical Parvalbumin-Positive Interneurons: A Canonical Microcircuit for Inhibition? J. Neurosci. *31*, 13260–13271. https://doi.org/10.1523/JNEUROSCI.3131-11.2011.
11. Fino, E., and Yuste, R. (2011). Dense inhibitory connectivity in neocortex. Neuron *69*, 1188–1203. https://doi.org/10.1016/j.neuron.2011.02.025.
12. Simons, D.J. (1978). Response properties of vibrissa units in rat SI somatosensory neocortex. J. Neurophysiol. *41*, 798–820. https://doi.org/10.1152/jn.1978.41.3.798.
13. Kerlin, A.M., Andermann, M.L., Berezovskii, V.K., and Reid, R.C. (2010). Broadly Tuned Response Properties of Diverse Inhibitory Neuron Subtypes in Mouse Visual Cortex. Neuron *67*, 858–871. https://doi.org/10.1016/j.neuron.2010.08.002.
14. Gabernet, L., Jadhav, S.P., Feldman, D.E., Carandini, M., and Scanziani, M. (2005). Somatosensory Integration Controlled by Dynamic Thalamocortical Feed-Forward Inhibition. Neuron *48*, 315–327. https://doi.org/10.1016/j.neuron.2005.09.022.
15. Cruikshank, S.J., Lewis, T.J., and Connors, B.W. (2007). Synaptic basis for intense thalamocortical activation of feedforward inhibitory cells in neocortex. Nat. Neurosci. *10*, 462–468. https://doi.org/10.1038/nn1861.
16. Isaacson, J.S., and Scanziani, M. (2011). How Inhibition Shapes Cortical Activity. Neuron *72*, 231–243. https://doi.org/10.1016/j.neuron.2011.09.027.
17. Haider, B., Häusser, M., and Carandini, M. (2013). Inhibition dominates sensory responses in the awake cortex. Nature *493*, 97–100. https://doi.org/10.1038/nature11665.
18. Gentet, L.J., Avermann, M., Matyas, F., Staiger, J.F., and Petersen, C.C.H. (2010). Membrane Potential Dynamics of GABAergic Neurons in the Barrel Cortex of Behaving Mice. Neuron *65*, 422–435. https://doi.org/10.1016/j.neuron.2010.01.006.
19. O'Connor, D.H., Peron, S.P., Huber, D., and Svoboda, K. (2010). Neural activity in barrel cortex underlying vibrissa-based object localization in mice. Neuron *67*, 1048–1061. https://doi.org/10.1016/j.neuron.2010.08.026.
20. Peron, S.P., Freeman, J., Iyer, V., Guo, C., and Svoboda, K. (2015). A Cellular Resolution Map of Barrel Cortex Activity during Tactile Behavior. Neuron *86*, 783–799. https://doi.org/10.1016/j.neuron.2015.03.027.
21. Crochet, S., Poulet, J.F.A., Kremer, Y., and Petersen, C.C.H. (2011). Synaptic mechanisms underlying sparse coding of active touch. Neuron *69*, 1160–1175. https://doi.org/10.1016/j.neuron.2011.02.022.
22. Brecht, M., Schneider, M., and Manns, I.D. (2005). Silent neurons in sensorimotor cortices: Implications for cortical plasticity. In Neural Plasticity in Adult Somatic Sensory-Motor Systems, F. Ebner, ed. (CRC Press), pp. 1–19.
23. Shoham, S., O'Connor, D.H., and Segev, R. (2006). How silent is the brain: is there a "dark matter" problem in neuroscience? J. Comp. Physiol. A Neuroethol. Sens. Neural Behav. Physiol. *192*, 777–784. https://doi.org/10.1007/s00359-006-0117-6.
24. Britten, K.H., Newsome, W.T., Shadlen, M.N., Celebrini, S., and Movshon, J.A. (1996). A relationship between behavioral choice and the visual responses of neurons in macaque MT. Vis. Neurosci. *13*, 87–100. https://doi.org/10.1017/S095252380000715X.
25. Newsome, W.T., Britten, K.H., and Movshon, J.A. (1989). Neuronal correlates of a perceptual decision. Nature *341*, 52–54. https://doi.org/10.1038/341052a0.
26. Sachidhanandam, S., Sreenivasan, V., Kyriakatos, A., Kremer, Y., and Petersen, C.C.H. (2013). Membrane potential correlates of sensory perception in mouse barrel cortex. Nat. Neurosci. *16*, 1671–1677. https://doi.org/10.1038/nn.3532.
27. Nienborg, H., Cohen, M.R., and Cumming, B.G. (2012). Decision-related activity in sensory neurons: Correlations among neurons and with

Neuron, Volume *112*

Supplemental information

A latent pool of neurons silenced by sensory-evoked inhibition can be recruited to enhance perception

Oliver M. Gauld, Adam M. Packer, Lloyd E. Russell, Henry W.P. Dalgleish, Maya Iuga, Francisco Sacadura, Arnd Roth, Beverley A. Clark, and Michael Häusser

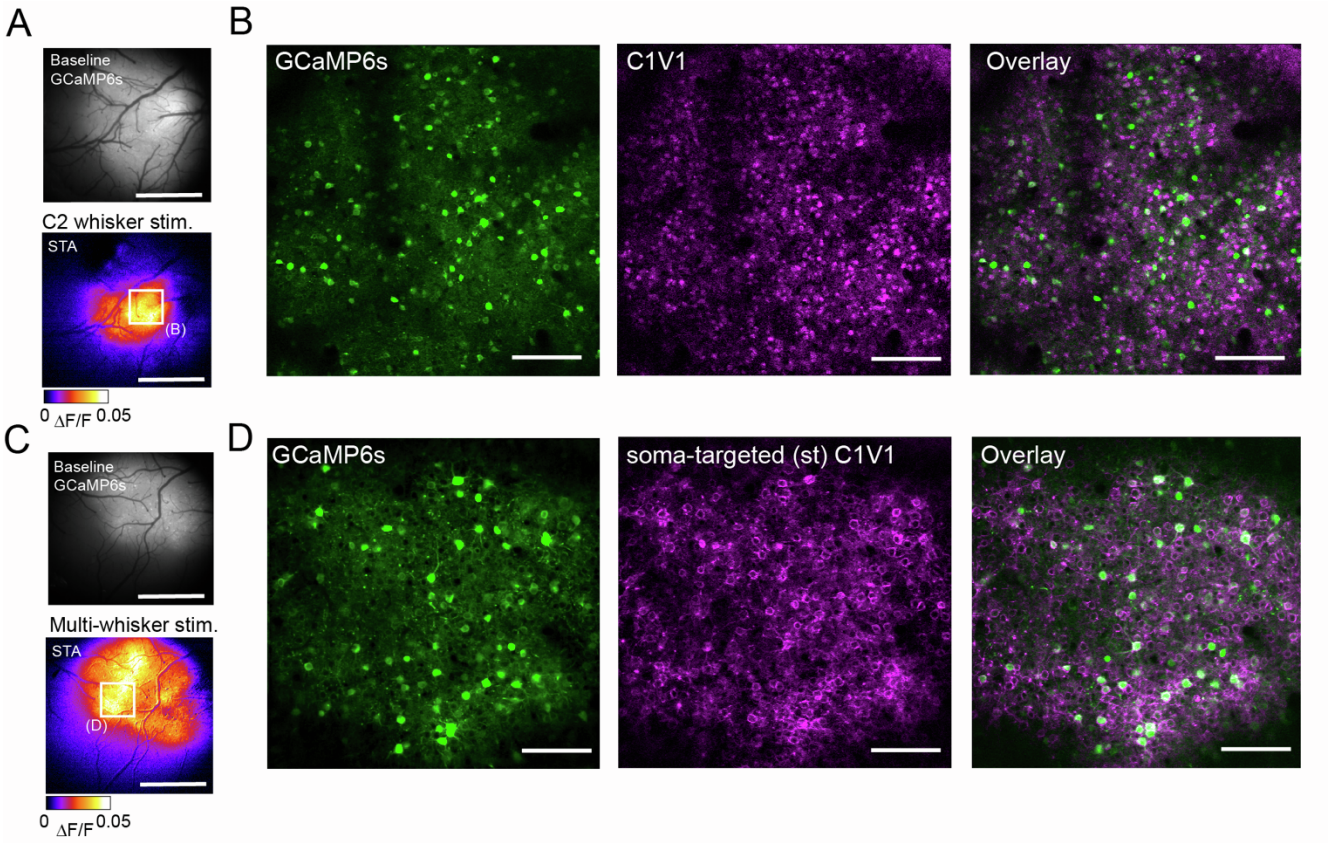

Figure S1. Co-expression of GCaMP6s and C1V1 in barrel cortex, related to Figures 1-4

(A) Localization of the C2 whisker barrel using widefield fluorescence imaging. Top image shows widefield baseline GCaMP6s fluorescence imaged through the cranial window. Bottom image shows the stimulus-triggered average (STA) fluorescence response following stimulation of the contralateral C2 whisker. The STA image shows the average ΔF/F response 0.5 - 1 s post stimulus. The white square indicates the location of the 2P field of view shown in panel (B). **(B)** 2P images of GCaMP6s (left, 920 nm) and C1V1-mCherry (middle, 765 nm) co-expression in L2/3 barrel cortex. The right image shows the overlay. **(C)** Same as (A) but showing the widefield cortical ΔF/F response 0.5 - 1 s after the simultaneous stimulation of multiple contralateral whiskers in a different example mouse. The white box indicates the FOV location in (D). **(D)** 2P images of GCaMP6s expression (left, 920 nm), st-C1V1-mScarlet expression (right, 765 nm) and the overlay (right) in L2/3 neurons in barrel cortex. Images in (D) correspond to the FOV depicted in Figure 3D. Scale bar for widefield images = 1 mm. Scale bar for 2P images = 100 µm.

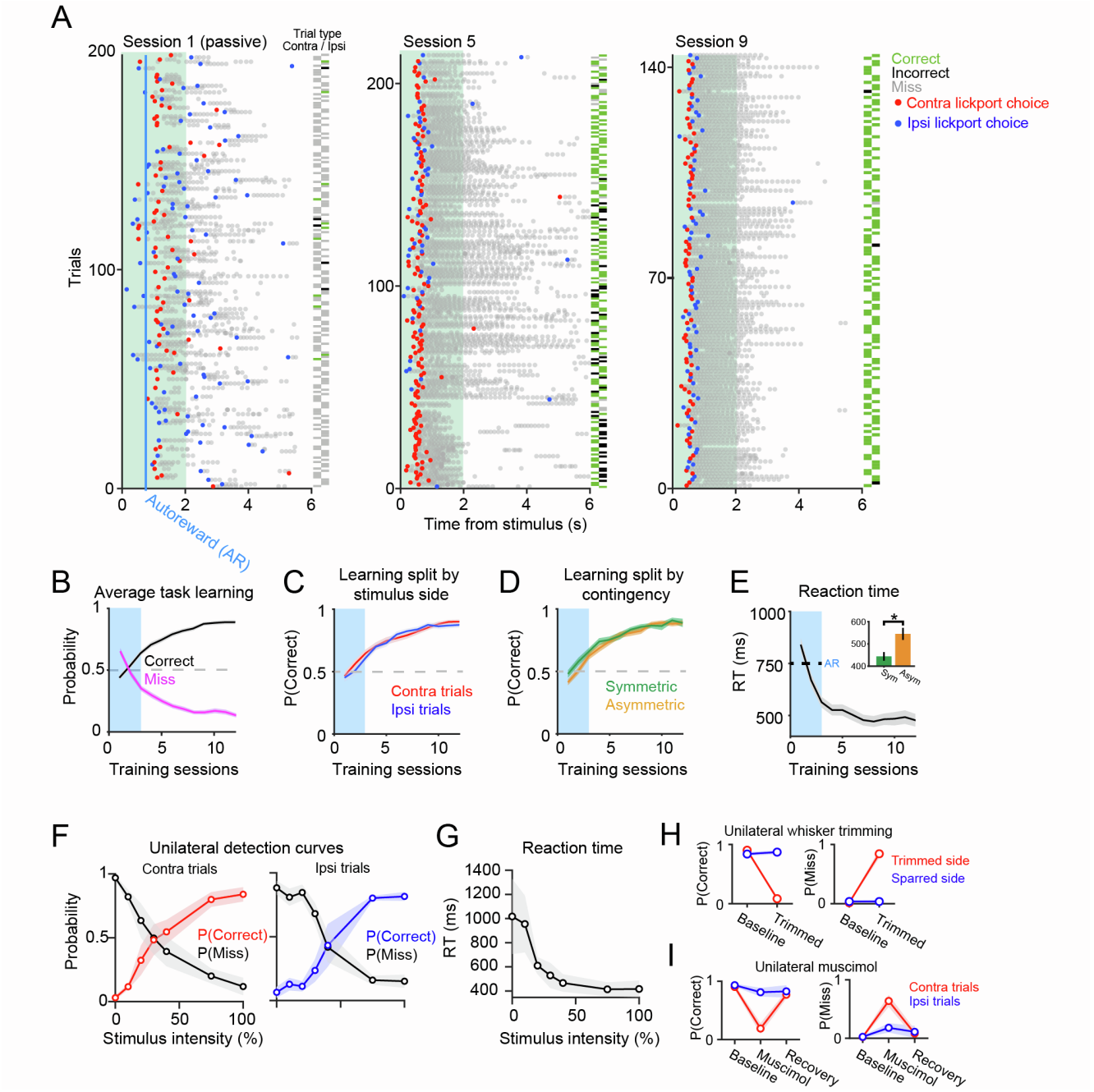

Figure S2. Task learning and behavioral control experiments, related to Figure 1

(A) Behavioral performance plots from an example animal in 3 different sessions across learning. The vertical blue line indicates the time of the autoreward (750 ms) - which was used to shape learning during early sessions. Each row corresponds to a trial, and each marker shows a lick. The first post-stimulus lick is coloured red/blue according to contra/ipsi lickport choice. Trial-type and trial outcome are indicated by the location and colour of the rectangular ticks on the right side of the session plot. **(B)** Average performance curves. P(Correct) and P(Miss) rate are shown in black and magenta across sessions. Data show the mean ± SEM across 61 mice; 259 ± 79 trials per session. **(C)** Average performance split by contra (red) and ipsi (blue) trials across learning. **(D)** Average performance for symmetric-trained mice (green; n = 31 mice) and asymmetric-trained mice (orange; n = 30 mice) across learning. **(E)** Average reaction times for correct trials across learning. The inset shows quantification of mean RT across symmetric and asymmetric mice (on sessions with P(Correct) > 70%). RT sym 448.2 ± 123.1 ms; mean ± std; asym 526.1 ± 220.3 ms, * $P < 0.05$ Wilcoxon rank-sum test. **(F)** Average performance ('P(Correct)') and miss rate across different unilateral deflection intensities for contra (left) and ipsi (right) stimulus trials. **(G)** Average reaction times across different deflection intensities. Data in F and G are from 4 mice (1 session per mouse). **(H)** Task performance before and after unilateral whisker trimming. Whisker trimming experiments were performed in 8 mice on the final day of experiments/training. P(Miss) *baseline* 0.02 ± 0.03; *trimmed whisker* 0.84 ± 0.19 mean ± std, *** $P < 0.0001$, Wilcoxon signed-rank test. P(Miss) *baseline* 0.04 ± 0.04, *spared whisker* 0.04 ± 0.07, n.s. $P > 0.05$. **(I)** Task performance before and 20 minutes after unilateral muscimol infusion in barrel cortex. Recovery performance was assessed 24 hours later. Muscimol experiments were performed in 4 mice (1 session per mouse) trained on the symmetric-contingency. P(Miss) *contra whisker baseline*: 0.02 ± 0.04, +*muscimol* 0.64 ± 0.2 mean ± std, ** $P < 0.01$. P(Miss) *ipsi whisker baseline* 0.02 ± 0.03, +*muscimol* 0.18 ± 0.16, n.s. $P > 0.05$. Statistical tests were Wilcoxon signed-rank tests, n = 4 mice.

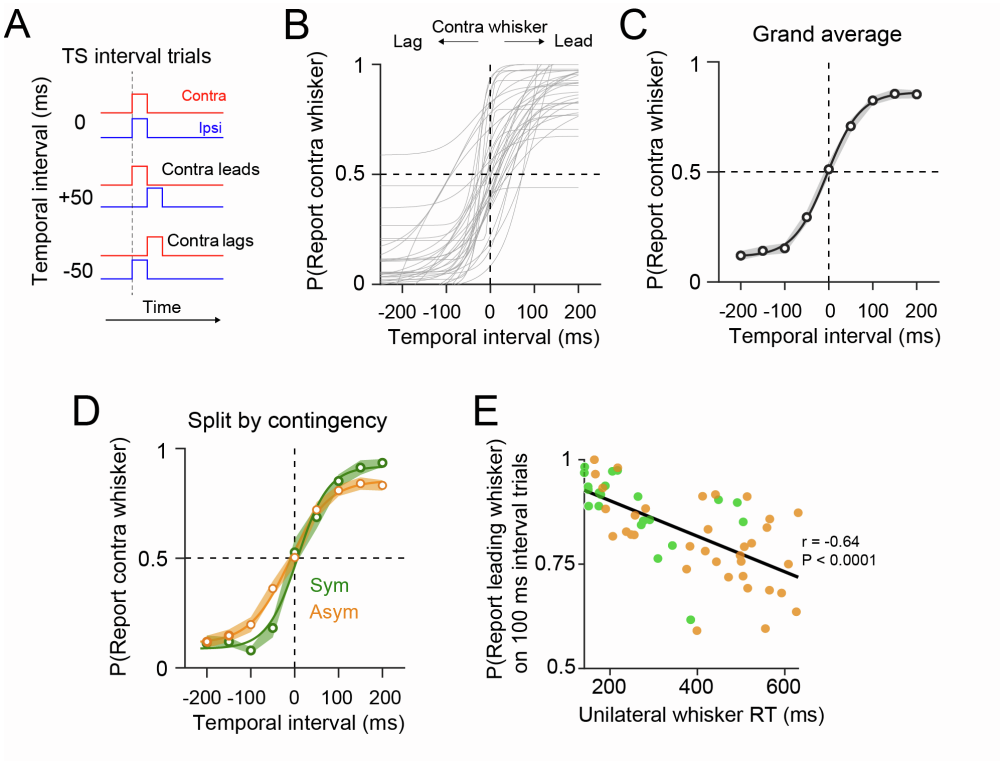

Figure S3. Temporal discrimination of bilateral whisker stimulation, related to Figure 1

(A) Schematic overview of threshold stimulus (TS) interval trials. The TS was defined during a short behavioral session as the bilateral stimulus that would give rise to chance performance. To probe temporal sensitivity to intervals in bilateral whisker stimulation mice received trials where the contra and ipsi component of the bilateral TS were offset in time. TS-interval trials were not rewarded and were interleaved with a high-proportion of unilateral trials to maintain task engagement. **(B)** Choice tendency 'P(Report contra whisker)' is shown as a function of bilateral whisker temporal interval. Each line represents a psychometric curve from an individual training session (n = 58 sessions, 25 mice). **(C)** Average temporal discrimination curve generated from the data in (B). **(D)** Average temporal discrimination curves are shown for symmetric (green) and asymmetric (orange) trained mice. **(E)** Leading whisker bias on 100 ms interval trials is plotted against mean reaction times on unilateral whisker trials. Individual points show single sessions from symmetric (green) and asymmetric (orange) trained mice (23 sessions in 9 symmetric, 35 sessions in 16 asymmetric mice).

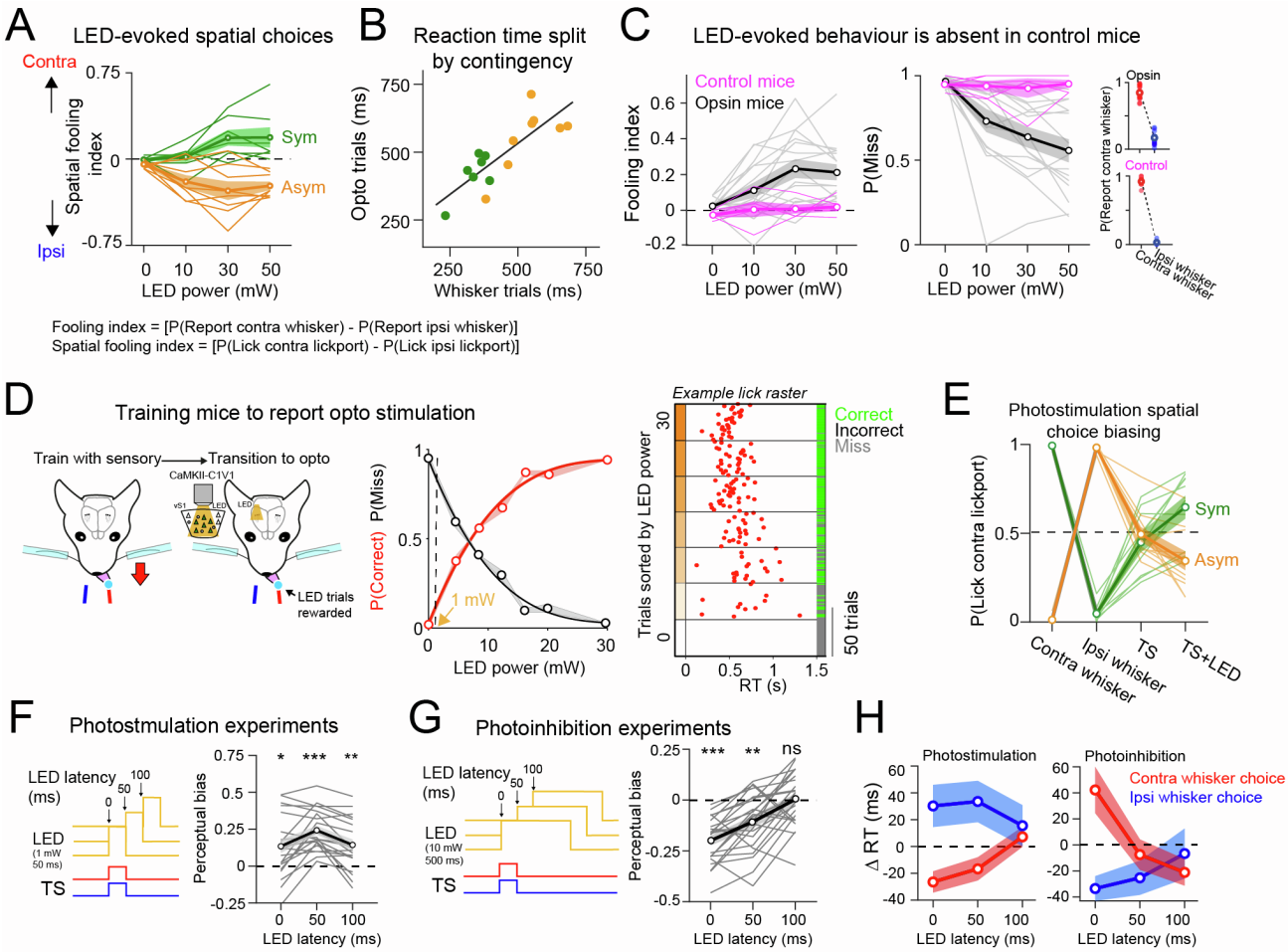

Figure S4. Optogenetic manipulation of task performance: additional analyses and control experiments, related to Figure 2

(A) Optogenetic 'substitution' experiments split by task contingency (n = 8 sessions in 4 symmetric-trained mice, and n = 8 sessions in 8 asymmetric-trained mice). **(B)** Average reaction time (RT) during optogenetic 'substitution' experiments showing symmetric (green) and asymmetric (orange) trained mice. Average RT on LED trials; sym = 421.1 ± 78.2 ms; asym = 555.2 ± 117.4 ms; * P = 0.03; Wilcoxon rank-sum test; **(C)** Optogenetic stimulation does not evoke perceptual responses in whisker trained control mice that do not express C1V1 (n = 5 sessions in 4 mice). Left: Fooling index for opsin expressing mice (grey) and control mice (magenta). Middle: Same as Left but showing P(Miss). Right: Summary of behavioral performance on whisker trials during the optogenetic experiment for opsin expressing mice (top) and control mice (bottom). **(D)** Perceptual detection of optogenetic stimulation. A subset of mice were trained on whisker trials, then transitioned to solely detecting LED stimulation. Licking responses on LED trials were rewarded, and so mice were motivated to detect LED stimulation. This experiment allowed us to identify a weak LED power condition (1 mW, indicated with the orange arrow) for optogenetic biasing experiments in Figure 2F. Data are from 2 mice (initially trained on the symmetric sensorimotor contingency). The lick raster plot shows an example optogenetic detection session. Contralateral lick reaction times are plotted as red circles. The LED power was modulated (0 – 30 mW, randomised) across different trials but sorted along the y- axis for display. **(E)** Spatial choice tendency during photostimulation-biasing sessions split by symmetric (green) and asymmetric (orange) trained mice. Symmetric-trained mice: ΔP(Lick contra lickport) = 0.2 ± 0.13; ** P = 0.004; Wilcoxon signed-rank test; n = 10 sessions, 8 mice. Asymmetric-trained mice: ΔP(Lick contra lickport) = -0.15 ± 0.14; ** P = 0.003; Wilcoxon signed-rank test; n = 11 sessions, 11 mice; **(F)** Left: Schematic overview of photostimulation biasing experiments. C1V1-expressing excitatory neurons were optogenetically stimulated with LED input (50 ms pulse duration), which was triggered at 0, 50 and 100 ms relative to the whisker Threshold Stimulus (TS). Right: Perceptual bias on TS+LED trials is shown for different LED latencies. **(G)** Left: Schematic overview of cortical photoinhibition biasing experiments. Unilateral photoinhibition was performed by activating PV interneurons expressing C1V1 with an LED. Photoinhibition was triggered at 0, 50 and 100 ms relative to the TS. Right same as in (F) but for perceptual biasing on photoinhibition experiments across LED latency trials. **(H)** Average reaction time biasing on photostimulation (left) and photoinhibition (right) biasing sessions across LED latency trials. Statistical tests were Wilcoxon signed rank tests; n.s. P > 0.05; * P < 0.05; ** P < 0.01; *** P < 0.001.

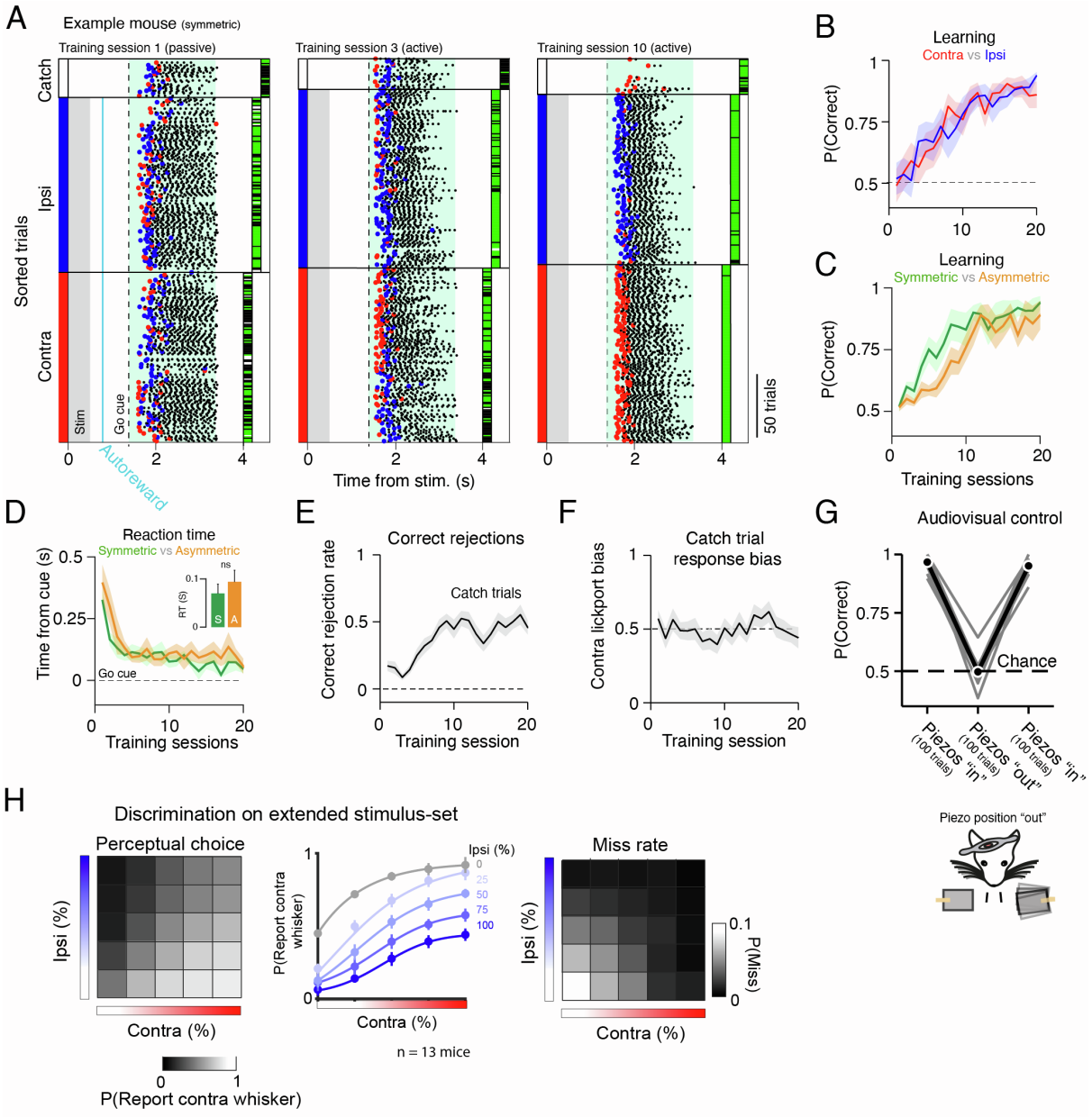

Figure S5. Behavioral data across delayed-response task learning, related to Figure 3

(A) Lick plots for an example symmetric-trained mouse across different stages of training. Trials are sorted along the y-axis according to stimulus type (contra, ipsi and catch). The blue vertical line in session 1 indicates the time of the programmed autoreward. Red/blue markers denote contra/ipsi lickport choice. The coloured ticks to the right of the axis denote correct (green), incorrect (black) and miss (white) trial outcomes. **(B)** Learning curves for contra (red) and ipsi (blue) trials. **(C)** Learning curves for symmetric (green, 7 mice) and asymmetric (orange, 6 mice) mice. Days to reach expert; sym = 8.14 ± 5; n = 7 mice; asym = 10 ± 1.6; n = 6 mice; n.s. P = 0.2; Wilcoxon ranked-sum test. **(D)** Average reaction times on correct trials across learning split by task contingency as in (C). Comparison was tested with a Wilcoxon rank sum test. n.s. P > 0.05. **(E)** Correct rejection rate on catch (no stimulus) trials across training. **(F)** Average response bias on catch trials across training. **(G)** Discrimination performance on unilateral trials was compared when the whisker deflector paddles were in contact with the whiskers (”in”), and when the paddles were positioned in an anterior position (”out”). This confirmed that mice do not sure audio-visual cues to solve the task. Individual grey lines show individual sessions. *P(Correct) baseline* = 0.97 ± 0.03 vs *paddles out of reach* = 0.5 ± 0.06; P < 0.0001; Wilcoxon signed-rank test; n = 13 mice. **(H)** Discrimination accuracy for bilateral discrimination sessions during training. During some training sessions, mice received 25 different stimulus combinations from a 5x5 stimulus matrix. Data in this figure are pooled across symmetric (7 mice) and asymmetric-trained (6 mice) mice.

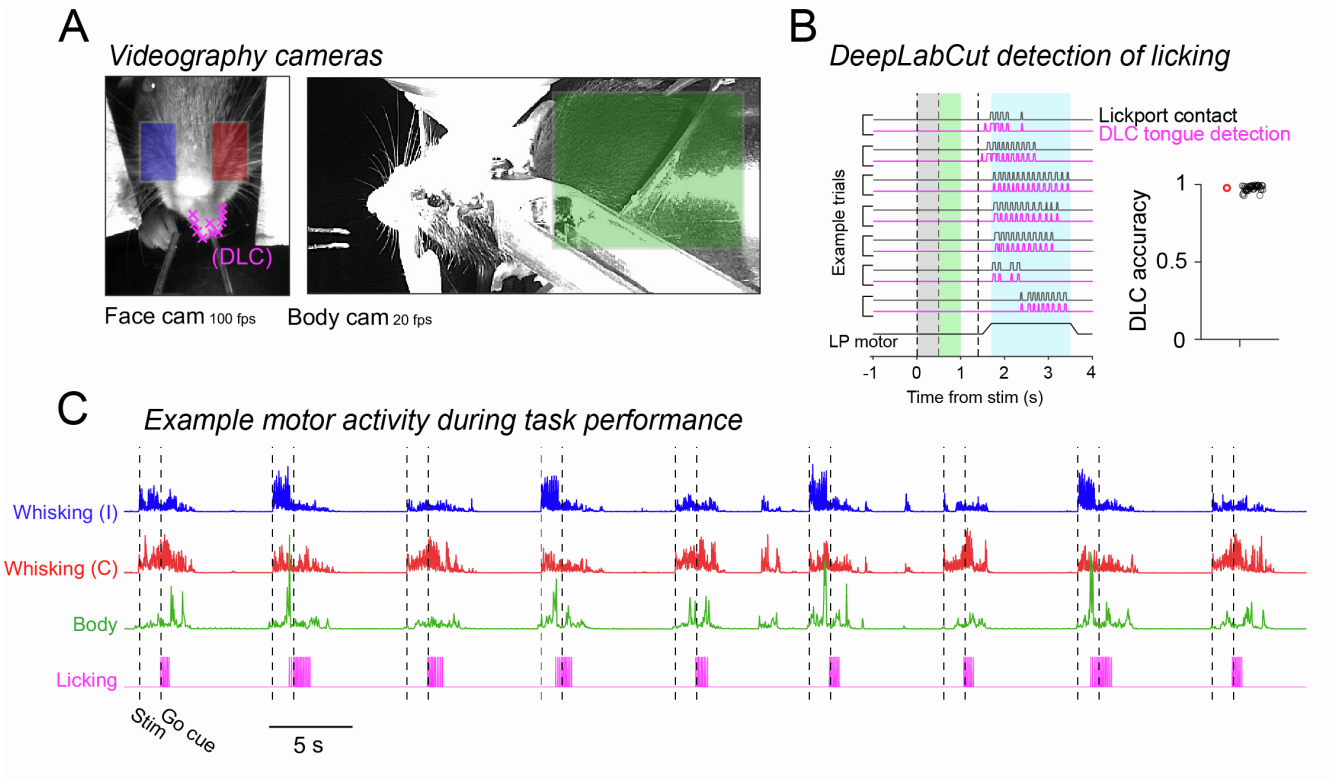

Figure S6. Characterising movements during task performance using behavioral videography, related to Figures 3 and 6

(A) Example images show the standard view from 2 cameras, one set to record facial activity (left), and another set to record body movements (right). The coloured rectangular boxes indicate ROIs positioned to extract whisker pad movements (blue, red) and body movements (green) during task performance. The magenta 'x' markers indicate DeepLabCut tracking points tracing the outline of the tongue. **(B)** Comparing video-detected licks (magenta) with electrical lickport-detected licks (black) on 7 example trials. The summary plot shows quantification accuracy of video-detected licks compared with 'ground truth' lickport-detect licks. The red marker shows the overall average, while the black circles show the average performance for each session (52 session in 13 mice). On average, DeepLabCut performed with high accuracy (~98%; mean accuracy across 52 session) at detecting the tongue during licking behavior. **(C)** Example whisking (red, blue), body movement (green) and licking (magenta) quantified using videography across a short section (9 trials) of continuous task performance.

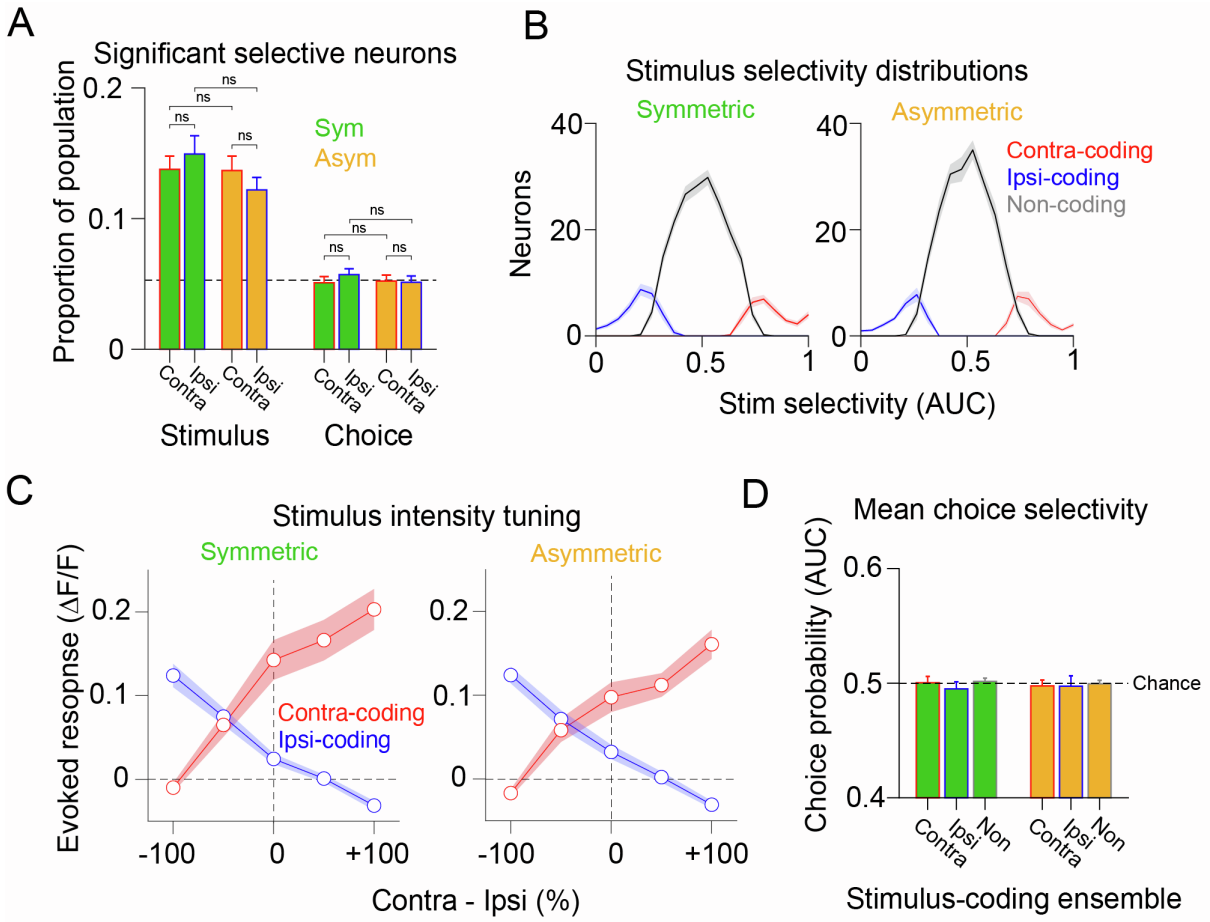

Figure S7. Task-evoked neural activity is comparable across symmetric and asymmetric contingencies, related to Figure 3

(A) The fraction of statistically significant stimulus and choice-selective neurons for symmetric (green; n = 30 sessions in 7 mice; 4.3 ± 2 sessions per mouse; mean ± std) and asymmetric-trained (orange; n = 22 sessions in 6 mice; 3.7 ± 1.8 sessions per mouse) mice. **(B)** Average distribution of stimulus-selectivity scores for symmetric (left) and asymmetric (right) trained mice. **(C)** Mean evoked response size across trial-types in stimulus coding ensembles for symmetric (left) and asymmetric-trained (right) mice. **(D)** Mean choice probability scores across stimulus-coding and non-coding ensembles for symmetric (green) and asymmetric-trained (orange) mice. Data in this figure are from 30 sessions in 7 symmetric-trained mice and 22 sessions in 6 asymmetric-trained mice. Average numbers of neurons per FOV: Symmetric 253.4 ± 44.7, Asymmetric 260.7 ± 43.9. Average ensemble size: contra-coding sym 36.2 ± 16 neurons; ipsi-coding sym 38.4 ± 18.8; non-coding sym 189.1 ± 37; contra-coding asym 37.3 ± 15.7 neurons; ipsi-coding asym 35.2 ± 17.1; non-coding asym 209.3 ± 35 (mean ± std). Statistical tests within contingency groups were Wilcoxon signed rank tests. Statistical tests across contingency groups were Wilcoxon rank sum tests. n.s. $P > 0.05$.

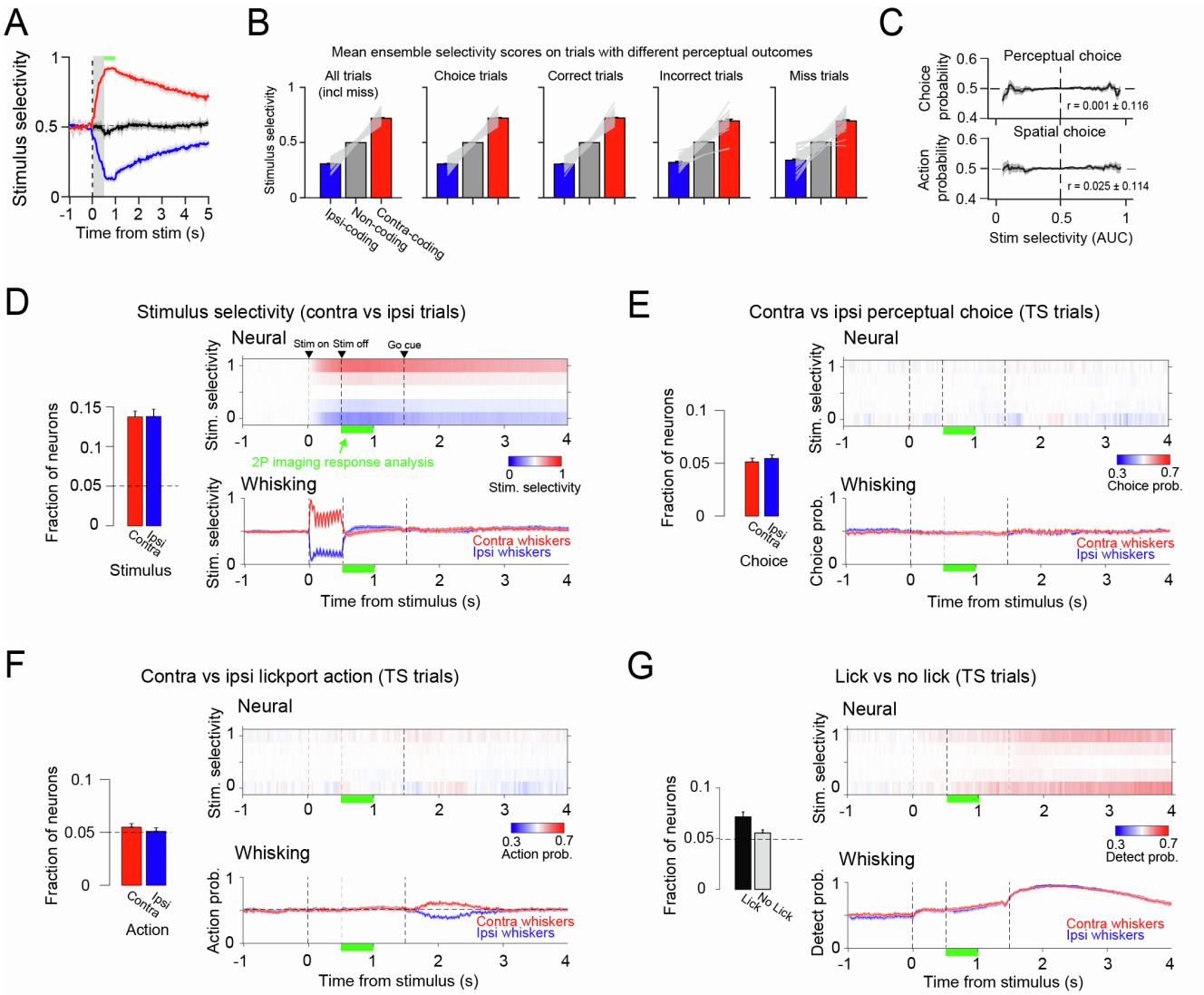

Figure S8. Stimulus-coding neurons do not predict behavioral choice, related to Figure 3

(A) Average stimulus-selectivity in contra-coding (red), ipsi-coding (blue) and non-coding (black) ensembles across the trial. **(B)** Average selectivity scores (during the response analysis window indicated by the green bar in (A)) on contra vs ipsi trials in ensemble groups split by trials with different behavioral outcomes. Individual grey lines show individual sessions, the coloured bars show the average across sessions. **(C)** Top: Summary of the correlation between stimulus-selectivity scores and choice probability (on TS trials) across all neurons in the FOV. The plot shows average CP scores in neurons binned by stimulus-selectivity. The line and error bars indicate the mean and SEM across all sessions. The mean correlation strength (Pearson's corr) across sessions is indicated on the plot. The bottom plot shows the same but for Action probability scores. **(D)** Overview of neural and whisking decoding of contra vs ipsi stimulus type. Bar plot: the average fraction of significantly selective stimulus-coding neurons in the FOV. The horizontal dashed line at 0.05 indicates chance (false pos. rate based on a $P < 0.05$ statistical threshold for detecting significant responses). Neural (top; heatmap colour shows neuronal stimulus-selectivity across time (x-axis) across all neurons binned by stimulus-selectivity scores (y-axis) across all 52 sessions) and whisker (bottom; traces show analysis of whisking from the contra and ipsi side of the snout) decoding of contra vs ipsi whisker trials is shown across the trial epoch. **(E)** Bar plot: the average fraction of significantly selective whisker-choice coding neurons in the FOV. Neural (top) and whisker (bottom) decoding of perceptual choice is shown across the trial-epoch. Average contra whisking CP during the delay epoch (green shading): 0.47 ± 0.12; n.s. P = 0.17; Average ipsi whisking CP during the delay epoch (green shading): 0.48 ± 0.11; n.s. P = 0.16; Wilcoxon signed-rank test difference tested against 0.5; **(F)** Bar plot: the average fraction of significantly selective lickport-choice coding neurons in the FOV. Neural (top) and whisker (bottom) decoding of lickport choice is shown across the trial-epoch. Average contra whisking AP during the delay epoch (green shading): 0.52 ± 0.12; n.s. P = 0.23; Average ipsi whisking AP during the delay epoch (green shading): 0.52 ± 0.11; n.s. P = 0.19; Wilcoxon signed-rank test difference tested against 0.5 **(G)** Bar plot: the average fraction of significantly selective 'lick' vs 'no lick' coding neurons in the FOV. Neural (top) and whisker (bottom) decoding of 'lick' vs 'no lick' trials is shown across the trial-epoch. Fraction of neurons significant for 'lick' trials: 0.07 ± 0.04; *** $P = 1.5 \times 10^{-4}$; Wilcoxon signed-rank test tested against 0.05; Average contra whisking DP during the delay epoch (green shading): 0.58 ± 0.02; *** $P = 4 \times 10^{-6}$; Average ipsi whisking DP during the delay epoch (green shading):: 0.56 ± 0.01; *** $P = 7.9 \times 10^{-4}$; Wilcoxon signed-rank test difference tested against 0.5; Data in this figure are from 52 sessions in 13 mice and show the average ± SEM across sessions.

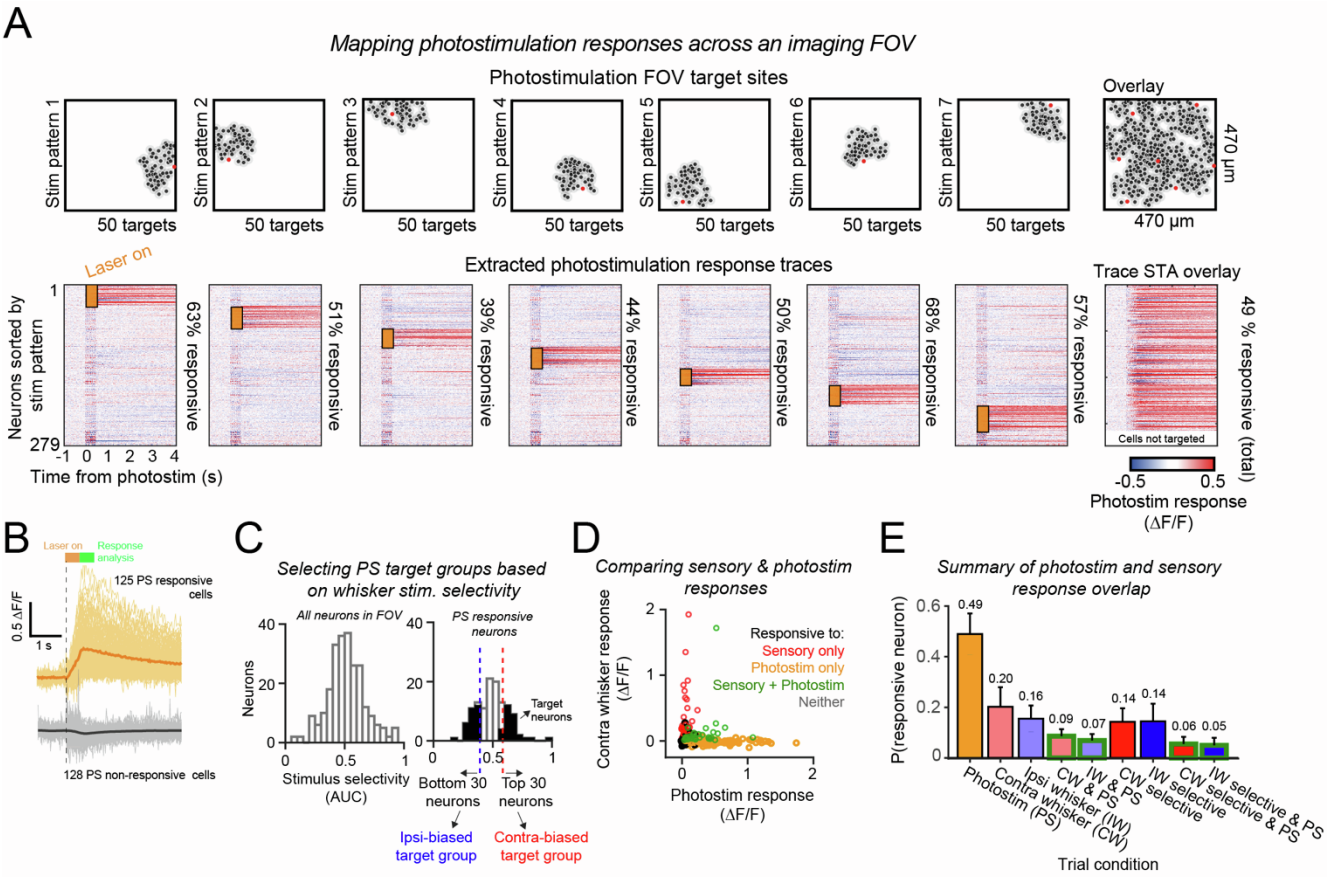

Figure S9. Selection of two-photon photostimulation target groups, related to Figure 4

(A) Example photostimulation mapping for an example experiment. All neurons in the FOV were tested for their response to photostimulation. xy pixel locations corresponding to locations of neural somata were detected semi-automatically and were clustered in 7 SLM stimulation patterns with 50 target sites per pattern. Top row: Each column relates to an individual SLM-target pattern within the FOV. The righthand column shows the combined overlay of all patterns. Each target image shows the spiral locations (15 µm diameter; black circle), with a target-zone proximity halo (40 µm diameter; grey circles). Red circles indicate the xy location of the photostimulation galvo mirrors, which were positioned to maximise SLM stimulation efficiency. Bottom row: Average photostimulation-triggered fluorescence traces are shown aligned to stimulation onset (0 s). The orange bars (0 – 0.5 s) indicate the neurons targeted in each stimulation pattern, and the duration of stimulation (500 ms). Neurons are sorted according to stimulation group along the y-axis. Stimulation of each SLM pattern selectively drives activity in the corresponding target neurons. The right image shows the overlay. Note the cells at the bottom of the 'overlay' heatmap were not identified as targets (distance from a spiral location > 20 µm). **(B)** Comparison of PS-evoked fluorescence traces of individual neurons in (A) identified as photostimulation-responsive (orange) and photostimulation non-responsive (black). Each trace shows the average response of a single neuron in (A) when the neuron was targeted for photostimulation. The average across all responsive and non-responsive neuron groups are shown as thicker lines. The green shaded bar indicates the window used to analysis PS responses (500 - 1000 ms post-stimulus onset). **(C)** Overview of target group selection process for an example session. Left: histogram showing whisker stimulus-selectivity scores across all neurons in the FOV. Right: histogram showing stimulus-selectivity scores of PS-responsive neurons in the FOV (as identified in B). Based on this result, photostimulation target groups were designed by selecting the 30 neurons at the top (contra biased) and bottom (ipsi biased) of the distribution. **(D)** Comparison of sensory and photostimulation responses across neurons in an example session. Individual marker points show individual neurons, and the colour denotes whether the neuron was significantly responsive to sensory and/or photostimulation (253 neurons). **(E)** Quantification of the average fraction of neurons significantly responsive to photostimulation and different sensory stimuli across all sessions (52 sessions, 13 mice). Note that finding photostimulation-responsive neurons with significant selectivity for contra vs ipsi whisker input was rare (~5%).

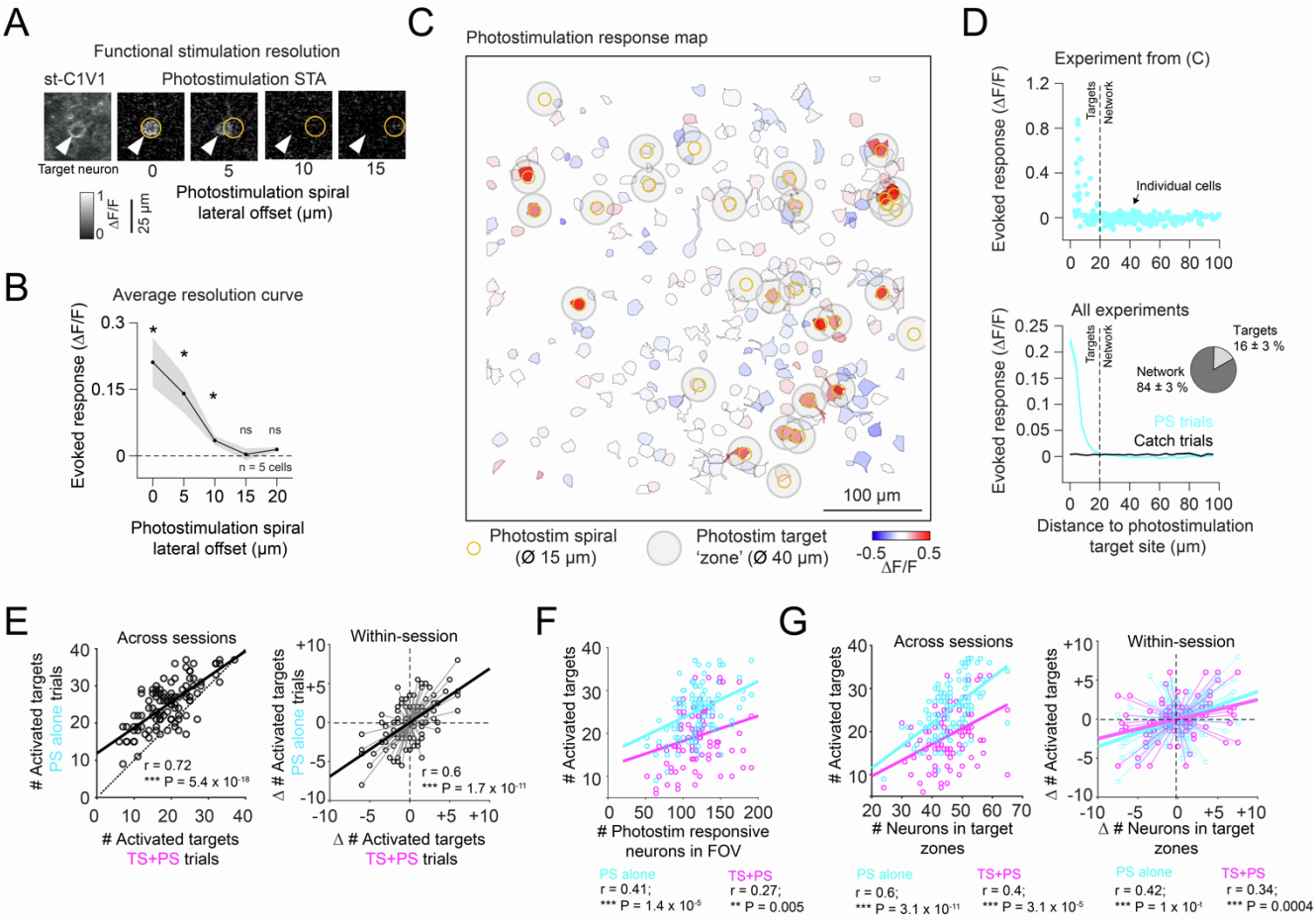

Figure S10. Functional resolution of targeted photostimulation, related to Figure 4

(A) Photostimulation resolution was assessed by measuring the fluorescence response (500 - 1000 post-stimulus) in a target neuron as the photostimulation spiral was offset laterally across the cell body. An example pixelwise STA at 0, 5, 10 and 15 µm offset is shown. The white arrow indicates the location of target cell, the orange dashed circle indicates the location of the PS spiral. **(B)** The average PS response of 5 cells as a function of spiral target-site offset as shown in (A). Statistical tests were Wilcoxon signed rank tests difference tested against 0; * P < 0.05. **(C)** Example map showing the photostimulation response for a single SLM-target neuron group (the FOV is the same as in Figure 3D and S1D). The smaller orange circles indicated the locations and size of photostimulation spirals in the FOV, the larger shaded grey circles indicate target 'zones', defined by functional stimulation resolution calibration. Neurons outside target zones ('network' cells), are unlikely to receive direct photo-stimulation. ROIs are segmented by Suite2p and coloured according to mean extracted fluorescence response on PS trials. **(D)** Top: average photostimulation responses extracted from ROIs in the example FOV shown in (C) plotted against distance to nearest photostimulation target site. Each cyan data point represents a single neuron (n = 246 neurons). Bottom: Average photostimulation vs distance to target site responses (binned along the x-axis) for all sessions (cyan). The response on catch trials is shown in dark grey (n = 52 sessions, 2 target-groups per sessions). The vertical dashed line at 20 um shows the target zone threshold. The inset shows the average proportion of target and network cells across all sessions (mean across 104 photostimulation conditions). **(E)** Left: Across session correlation between the number of activated targets on in the presence (x-axis) and absence (y-axis) of sensory (TS) input. Correlation is based on 104 photostimulation conditions (shown as individual markers) in 52 sessions. Right: Correlation between variability in the number of activated targets across the two photostimulation groups (within the same FOV) in the presence (x-axis) and absence (y-axis) of TS input. The data were mean-centred as described in Figure 5E. The correlation coefficient and p-value are indicated on the plot. **(F)** Correlation between the total number of PS-responsive neurons in the FOV (x-axis) and the number of activated targets on PS (cyan) and TS+PS (magenta) trials. **(G)** Right: Comparison between the total number of neurons within photostimulation target zones (x-axis) and the number of activated targets on PS (cyan) and TS+PS (magenta) trials across sessions. Left. Same as Right but showing the comparison across target groups within the same FOV. In all correlation plots, the thick line(s) shows the least-squares fit. The correlation strength (Pearson's corr) and p-value are indicated on the plot. Analyses were based on 104 photostimulation conditions in 52 sessions.

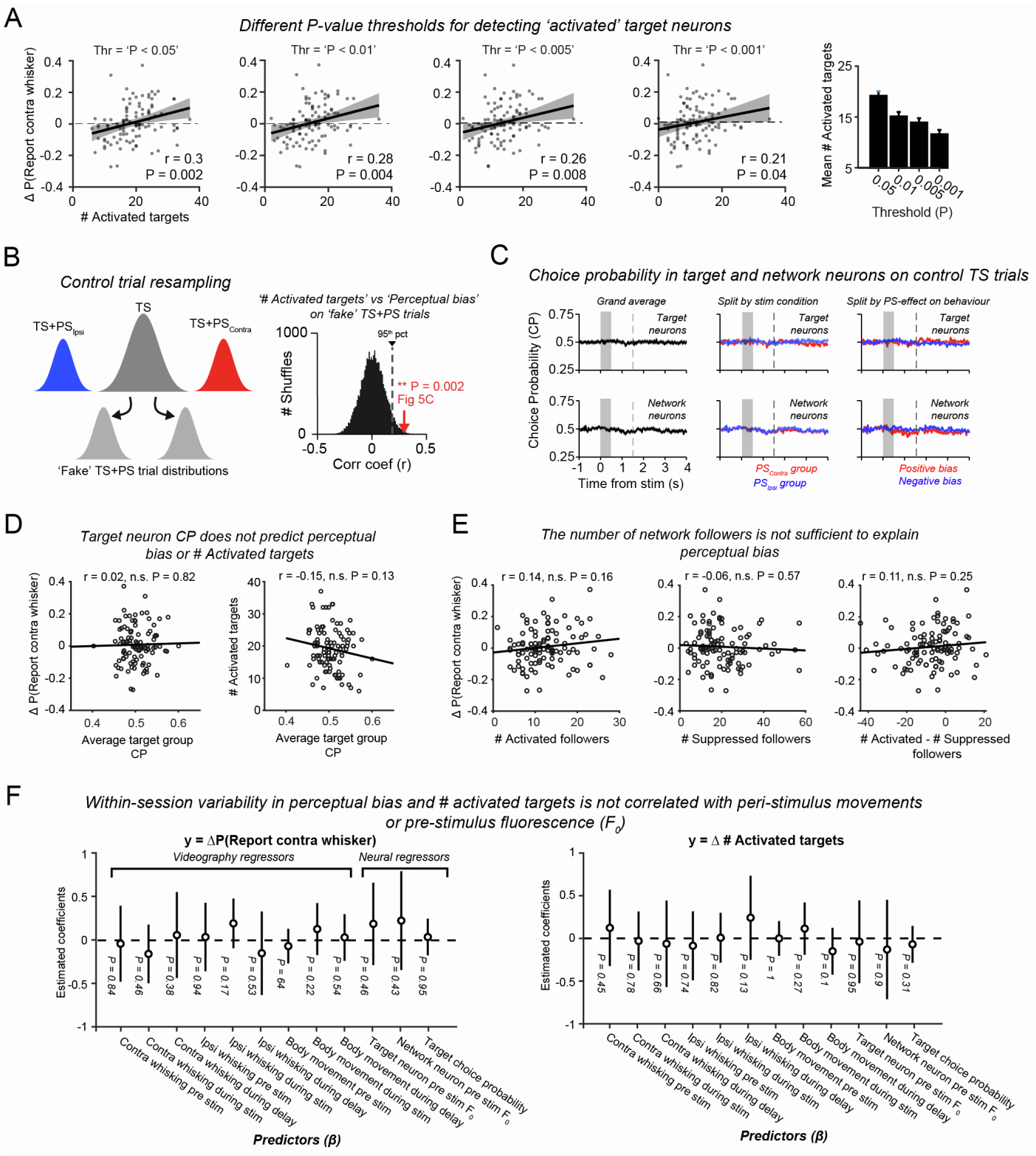
A
Different P-value thresholds for detecting 'activated' target neurons
Thr = 'P < 0.05'
Thr = 'P < 0.01'
Thr = 'P < 0.005'
Thr = 'P < 0.001'
Δ P(Report contra whisker)
# Activated targets
r = 0.3
P = 0.002
r = 0.28
P = 0.004
r = 0.26
P = 0.008
r = 0.21
P = 0.04
Mean # Activated targets
Threshold (P)
B
Control trial resampling
TS
TS+PS Ipsi
TS+PS Contra
'Fake' TS+PS trial distributions
'# Activated targets' vs 'Perceptual bias' on 'fake' TS+PS trials
95th pct
** P = 0.002
Fig 5C
Shuffles
Corr coef (r)
C
Choice probability in target and network neurons on control TS trials
Grand average
Split by stim condition
Split by PS-effect on behaviour
Target neurons
Network neurons
Choice Probability (CP)
Time from stim (s)
PS Contra group
PS Ipsi group
Positive bias
Negative bias
D
Target neuron CP does not predict perceptual bias or # Activated targets
r = 0.02, n.s. P = 0.82
r = -0.15, n.s. P = 0.13
Δ P(Report contra whisker)
Activated targets
Average target group CP
E
The number of network followers is not sufficient to explain perceptual bias
r = 0.14, n.s. P = 0.16
r = -0.06, n.s. P = 0.57
r = 0.11, n.s. P = 0.25
Δ P(Report contra whisker)
Activated followers
Suppressed followers
Activated - # Suppressed followers
F
Within-session variability in perceptual bias and # activated targets is not correlated with peri-stimulus movements or pre-stimulus fluorescence (F0)
y = ΔP(Report contra whisker)
Videography regressors
Neural regressors
Estimated coefficients
P = 0.84
P = 0.46
P = 0.38
P = 0.94
P = 0.17
P = 0.53
P = 64
P = 0.22
P = 0.54
P = 0.46
P = 0.43
P = 0.95
Contra whisking pre stim
Contra whisking during stim
Contra whisking during delay
Ipsi whisking pre stim
Ipsi whisking during stim
Ipsi whisking during delay
Body movement pre stim
Body movement during stim
Body movement during delay
Target neuron pre stim F0
Network neuron pre stim F0
Target choice probability
Predictors (β)
y = Δ # Activated targets
P = 0.45
P = 0.78
P = 0.66
P = 0.74
P = 0.82
P = 0.13
P = 1
P = 0.27
P = 0.1
P = 0.95
P = 0.9
P = 0.31

Figure S11. The correlation between activated targets and perceptual bias is not explained by other neural and behavioral factors, related to Figure 5

(A) Correlation plots showing perceptual bias (y-axis) against the number of activated target neurons (x-axis) when using different p-value thresholds for detecting activated targets. The correlation strength and significance is indicated on each plot. The plot on the far right shows the average number of neurons identified as significantly activated as a function of p-value thresholds. Correlations are based on 104 photostimulation conditions in 52 sessions. Shaded error bars show 95% confidence intervals of the linear regression fit. **(B)** Left: Schematic overview of the procedure for resampling TS control trials. Right: Distribution of the correlation coefficients (Pearson's corr r) obtained across 10000 iterations of the shuffled resampling procedure. The probability of obtaining a correlation r = 0.3 (as in Figure 5C) across sessions between target activation and perceptual bias on control trials was 0.002 (indicated by the red arrow). **(C)** Average choice probability in target groups (top row) and network neuron groups (bottom row) across sessions. The left column shows the grand average, the middle column shows groups split by contra vs ipsi-biased target group, and the right column shows target groups split by positive vs negative perceptual bias effect. **(D)** Target group choice probability does not correlate with perceptual bias (left), or with the number of activated target group neurons (right). The correlation strength (Pearson's corr) and significance is indicated on each plot. **(E)** The number of activated (left), suppressed (middle) or difference between activated and suppressed (right) followers does not predict the perceptual effect of PS on choice bias. **(F)** Summary results of a multiple linear regression analysis testing the relationship between within-session variability in perceptual bias (left) and within-session variability in target activation (right) and differences in number of behavioral and neural predictors measured across the two photostimulation groups. Behavioral predictors included quantification of pre (-1000 to 0 ms), during (0 to 500 ms) and post (500 to 1000 ms) stimulus whisking and body movement. Neural predictors included average pre-stimulus (-1000 to 0 ms) baseline F_0 fluorescence in target and network neurons groups and target group choice probability. Marker points show the estimated coefficients and 95% confidence intervals, with the p-values denoting significance of each predictor. Data in this figure come from n = 104 target groups across 52 sessions in 13 mice.

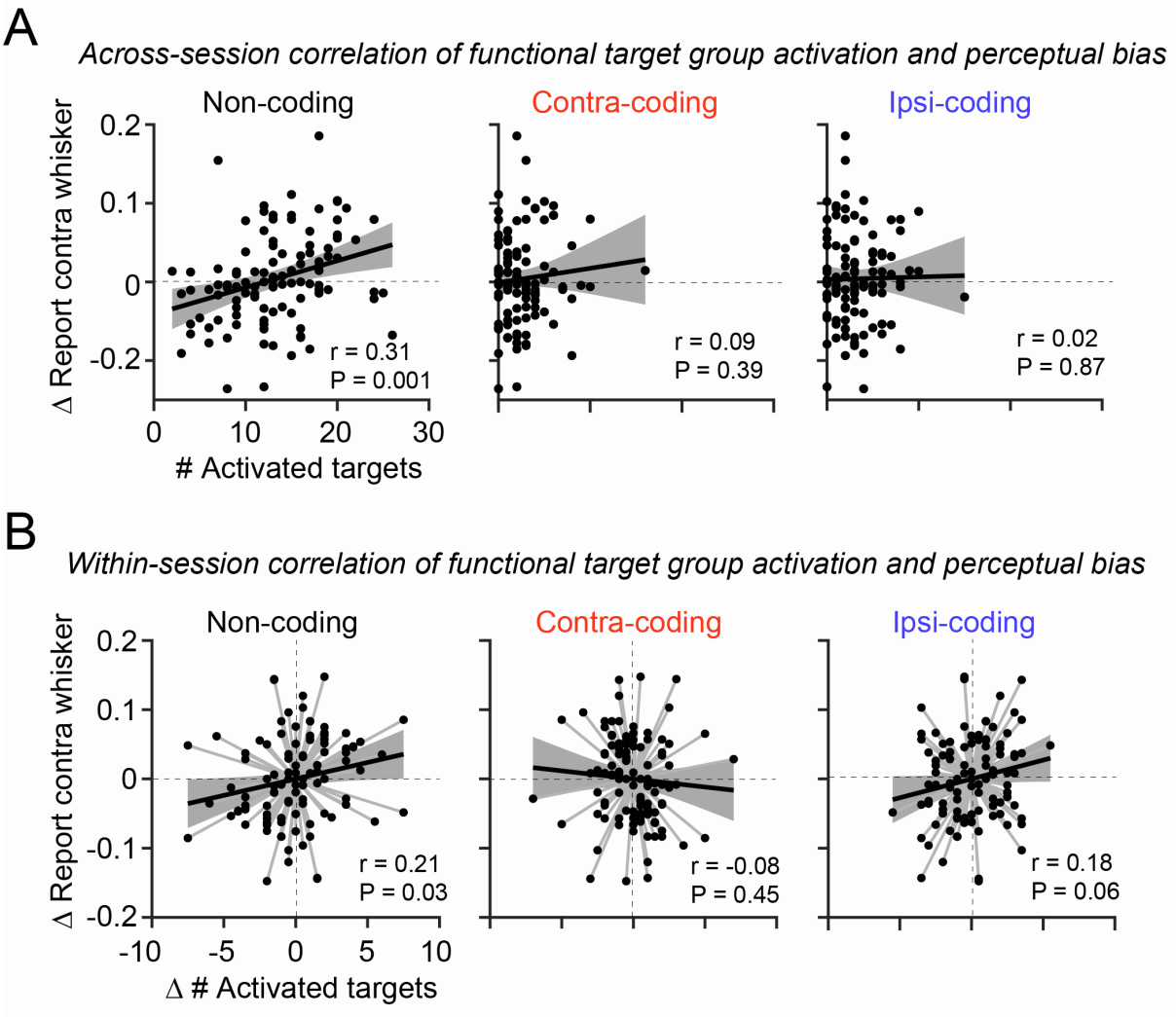

Figure S12. The number of non-coding targets activated predicts perceptual bias across and within sessions, related to Figure 6

(A) Perceptual bias (y-axis) is plotted against the number of activated targets (x-axis) in non-coding (left), contra-coding (middle) and ipsi-coding (right) categorical groups across sessions. The line and shaded error bars show the regression fit and 95% confidence intervals. The correlation strength (Pearson's corr) and significance are shown in each plot. **(B)** Same as (A) but showing the within-session comparison between photostimulation groups. Data come from 104 photostimulation conditions in 52 sessions. Each marker indicates an individual photostimulation condition.

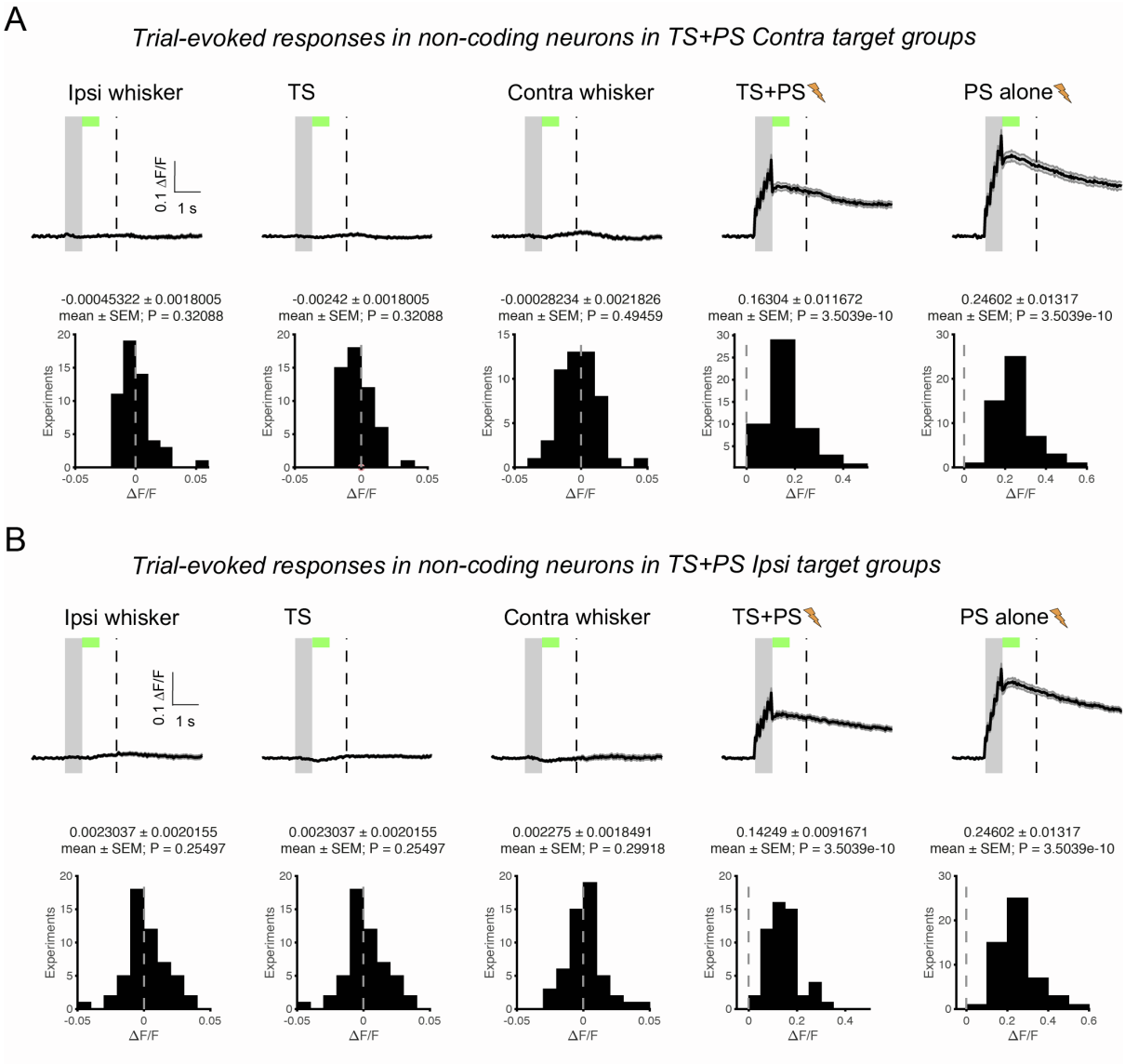

Figure S13. Trial-evoked activity in non-coding target neurons split by photostimulation target group, related to Figure 6

(A) Top row: Average evoked fluorescence traces in non-coding target neurons within the contra-biased PS target group across trial types (as shown in Figure 6). The grey shaded bar shows the stimulus presentation period, and the vertical dashed line shows the time of the go cue. Bottom row: Histogram of average evoked response in the non-coding target group (quantified 500 - 1000 ms post stimulus; green shaded bar in top row) is shown for all sessions (n = 52 sessions; 13 mice). The average response across all sessions in stated in the header text of each plot and the P-value shows the result of a Wilcoxon signed rank test comparing the distribution to 0. **(B)** same as in (A) but showing quantification of responses in non-coding neurons within the ipsi-biased PS target groups.